PHOTOPRODUCTION OF POSITIVE K-MESONS IN HYDROGEN AT LARGE CENTER OF MASS ANGLES

Thesis by

Melvin Drew Daybell

In Partial Fulfillment of the Requirements

For the Degree of

Doctor of Philosophy

California Institute of Technology

Pasadena, California

1962

ABSTRACT

This is the first of a series of experiments designed to take advantage of the extension of the peak energy of the Caltech electron synchrotron into the 1500 mev region to measure K-photoproduction in hydrogen at energies significantly above threshold. Data on both the $\gamma + p \rightarrow K^+ + \Lambda^\circ$ and the $\gamma + p \rightarrow K^+ + \Sigma^\circ$ reactions were obtained for photon energies from 1000 to 1400 mev and center of momentum angles near 125°. At the low energy limit of these measurements agreement is found with earlier measurements in this laboratory and at Cornell. In the 1100 to 1400 mev region the $K^+ + \Lambda^\circ$ differential production cross section appears to level off at a value of about 1.2×10^{-31} cm^2/steradian or possibly decrease slightly. The three $K^+ + \Sigma^\circ$ points taken continue the steep rise above threshold observed earlier at Cornell and then appear to drop off above 1250 mev.

The experiment was performed by allowing the K^+ particles produced in a liquid hydrogen target by the incident photon beam to pass through a symmetric wedge magnet, which focused the particles of the proper momentum onto a scintillation counter telescope in which they came to rest. In this way, the momentum, range, and specific ionization loss of each particle passing through the system was determined. To discriminate against the much more numerous pions and protons present, the velocity of each particle was measured by using time of flight techniques.

ACKNOWLEDGEMENTS

The active assistance of Dr. Matthew Sands in planning and performing the work described here was indispensible. His supervision and constant encouragement throughout the span of the author's graduate career were deeply appreciated.

Dr. R. F. Bacher was director of the laboratory during the performance of this experiment, and his presence was felt in many ways. The interest of Dr. R. L. Walker and Dr. A. V. Tollestrup in this work proved valuable on many occasions.

Dr. J. H. Mullins and Mr. Edward Taylor, and other members of the Synchrotron Laboratory staff offered valuable assistance on innumerable occasions.

Mr. Richard Talman and Mr. Robert Macek spent many hours helping to take and reduce data. Dr. Walter Wales built much of the equipment used, and was responsible for many of the features of the experimental method. Dr. R. Gomez was responsible not only for calibrating the beam monitoring system, but also for introducing the author to many of the tricks of experimental technique.

Numerous discussions with Mr. D. Groom, Mr. C. Peck, and Mr. H. Ruderman were invaluable.

It would have been impossible to accumulate the large amount of synchrotron operating time needed without the work of Mr. Dan Sell, Mr. Larry Loucks, and the rest of the synchrotron crew.

The financial support of the U. S. Atomic Energy Commission, the National Science Foundation, and my wife, is gratefully acknowledged.

TABLE OF CONTENTS

LIST OF ILLUSTRATIONS

I. INTRODUCTION

In 1947, a few months after the discovery of the long sought meson of Yukawa in nuclear emulsions, evidence was presented which suggested the existence of still more types of unstable particles. During the years that followed, the list of "elementary" particles grew until it included a whole new class of these so-called "strange" particles, exhibiting properties shared by none of the older types. It was soon learned that one of these new particles was produced only in association with another such particle, and never alone or in combination with only "old" particles. Not only that, although these "strange" particles were produced quite readily, and therefore would be expected to decay quickly by the same type of interactions that caused their production, their lifetimes were found to be quite long.

In 1955, by generalizing the concept of isotopic spin to include a new quantum number (strangeness) for every strongly interacting particle, Gell-Mann and Nishijima were able to produce a very simple and successful phenomenological theory to explain the associated production of the strange particles, as well as their long lifetimes. In addition, the existence of several particles that had not been discovered at that time was predicted by this theory. All but two of these have since been observed.

Prominent among these strange particles are the K meson and the Λ and Σ hyperons. These are the most

readily accessible to experiment, and have been the most thoroughly studied. One potentially fruitful avenue of approach to the interactions of these particles is through the study of the photoproduction reactions:

$$\gamma + p \rightarrow \Lambda^\circ + K^+ \quad (1)$$

$$\gamma + p \rightarrow \Sigma^\circ + K^+ \quad (2)$$

$$\gamma + n \rightarrow \Sigma^- + K^+ \quad (3)$$

$$\gamma + p \rightarrow K^\circ + \Sigma^+ \quad (4)$$

$$\gamma + n \rightarrow K^\circ + \Lambda^\circ \quad (5)$$

$$\gamma + n \rightarrow K^\circ + \Sigma^\circ \quad (6)$$

(Photoproduction of K^- from free nucleons requires much higher energies, since either a K^+ or a baryon-antibaryon pair must be produced at the same time.) These reactions have the advantage from the theoretical point of view that the properties of the electromagnetic interaction are fairly well understood, so that in photoproduction one comes close to being able to study the properties of the K mesons and the hyperons themselves. For example, with enough sufficiently accurate photoproduction data, the parity of the K meson with aspect to the nucleon-hyperon system may be determined.

For these and other reasons, much interest has been exhibited in K photoproduction in the years since 1956, when accelerators capable of supplying photons of energies high enough to

produce K's were first available. All of the published experimental work on these reactions to date has been done either at Caltech or at Cornell University (1-10). Only reactions (1) and (2) have been studied to any great extent, although some information on (3) has been obtained recently at Cornell by studying photoproduction from deuterium. A summary of the points at which differential production cross sections for reactions (1) and (2) have been measured is presented in figures 1 and 2.

The general features shown by these measurements are: for the Λ° production process the cross section increases approximately linearly with center of mass momentum to a value of about 1.5×10^{-31} cm^2/steradian at 1000 mev photon energy; this cross section is also isotropic up to about this energy, so that S-wave production is indicated; beyond 1000 mev the angular distribution is beginning to peak somewhat in the forward direction, and the cross section increases less rapidly with energy; in the Σ° production reaction, less data is available and all of it is for center of mass momenta greater than 150 mev; this data seems to indicate a cross section of about 0.9×10^{-31} cm^2/steradian containing a large P-wave component (8, 9). Results from the deuteron experiments give cross sections from 0.8 to 1.6 times the values for the $\gamma + p \rightarrow K^+ + \Sigma^\circ$ reaction, within rather large errors at present.

The present experiment was designed to obtain data at large center of mass angles where, because of unfavorable kinematic factors and a relatively higher pion background, few measurements had been made; and also to extend the range of measurement into the unexplored region above 1100 mev photon energy. Since the maximum momentum accepted by the spectrometer used was rather low, data were taken only at far backward angles, even at these higher energies.

The method used is essentially a combination of the techniques used earlier by Donoho and Walker (2) and by Brody, Wetherell, and Walker (5), and will be described in Chapter II.

FIGURE 1

POINTS AT WHICH CROSS SECTIONS FOR THE PROCESS

$\gamma + p \rightarrow K^+ + \Lambda^\circ$ HAVE BEEN REPORTED

The center of mass angle of the K meson and laboratory photon energy are shown for each point. Also shown are a few lines of constant K laboratory angle, θ_K, and K laboratory momentum, P_K. An arrow indicates the production threshold energy.

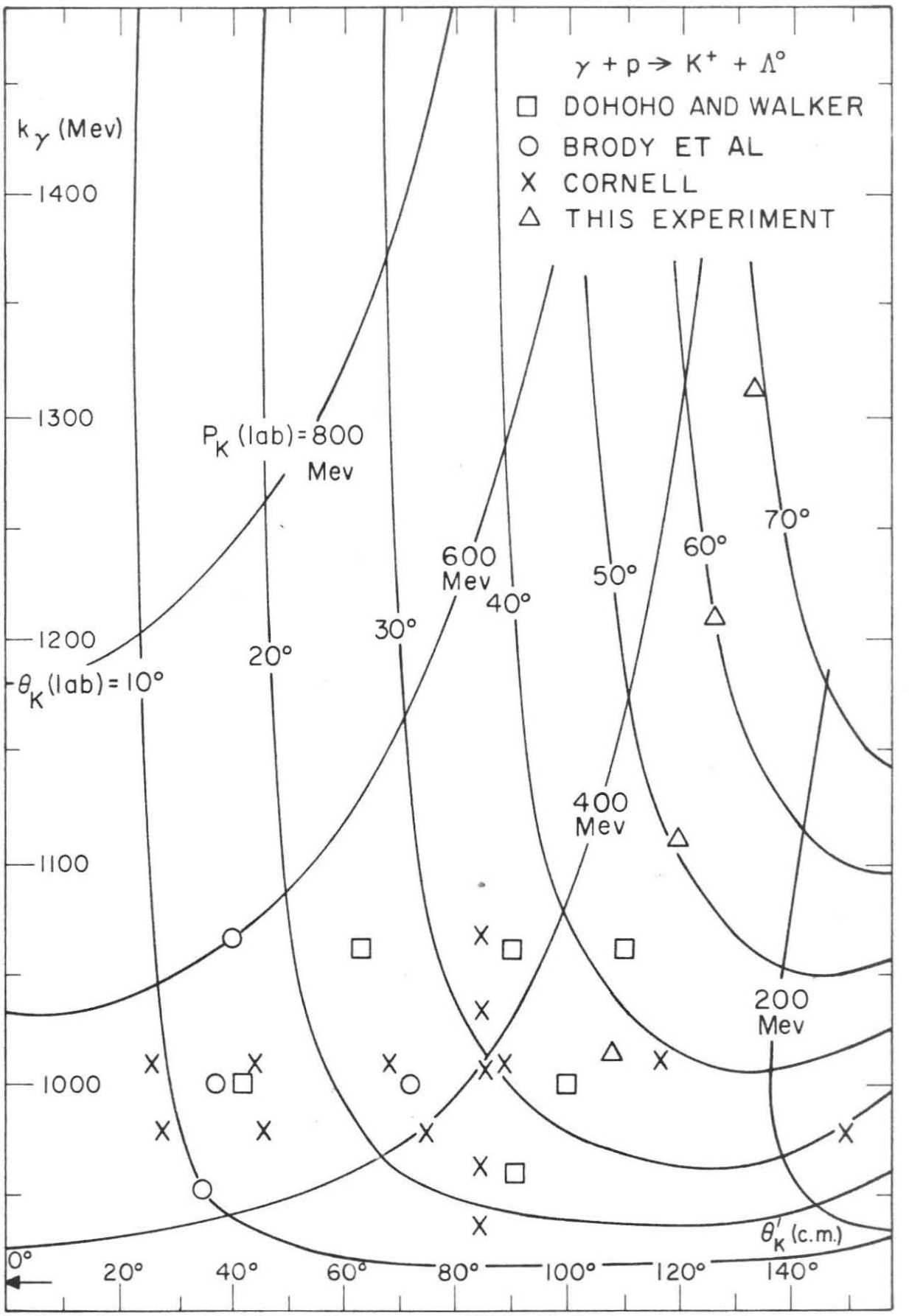
$\gamma + p \rightarrow K^+ + \Lambda^\circ$
DOHOHO AND WALKER
BRODY ET AL
CORNELL
THIS EXPERIMENT
k_γ (Mev)
1400
1300
1200
1100
1000
P_K (lab) = 800 Mev
600 Mev
400 Mev
200 Mev
θ_K (lab) = 10°
20°
30°
40°
50°
60°
70°
θ'_K (c.m.)
0°
20°
40°
60°
80°
100°
120°
140°

FIGURE 2

POINTS AT WHICH CROSS SECTIONS FOR THE PROCESS

$\gamma + p \rightarrow K^+ + \Sigma^\circ$ HAVE BEEN REPORTED

The center of mass angle of the K meson and laboratory photon energy are shown for each point. Also shown are a few lines of constant K laboratory angle, θ_K, and K laboratory momentum, P_K. An arrow indicates the production threshold energy.

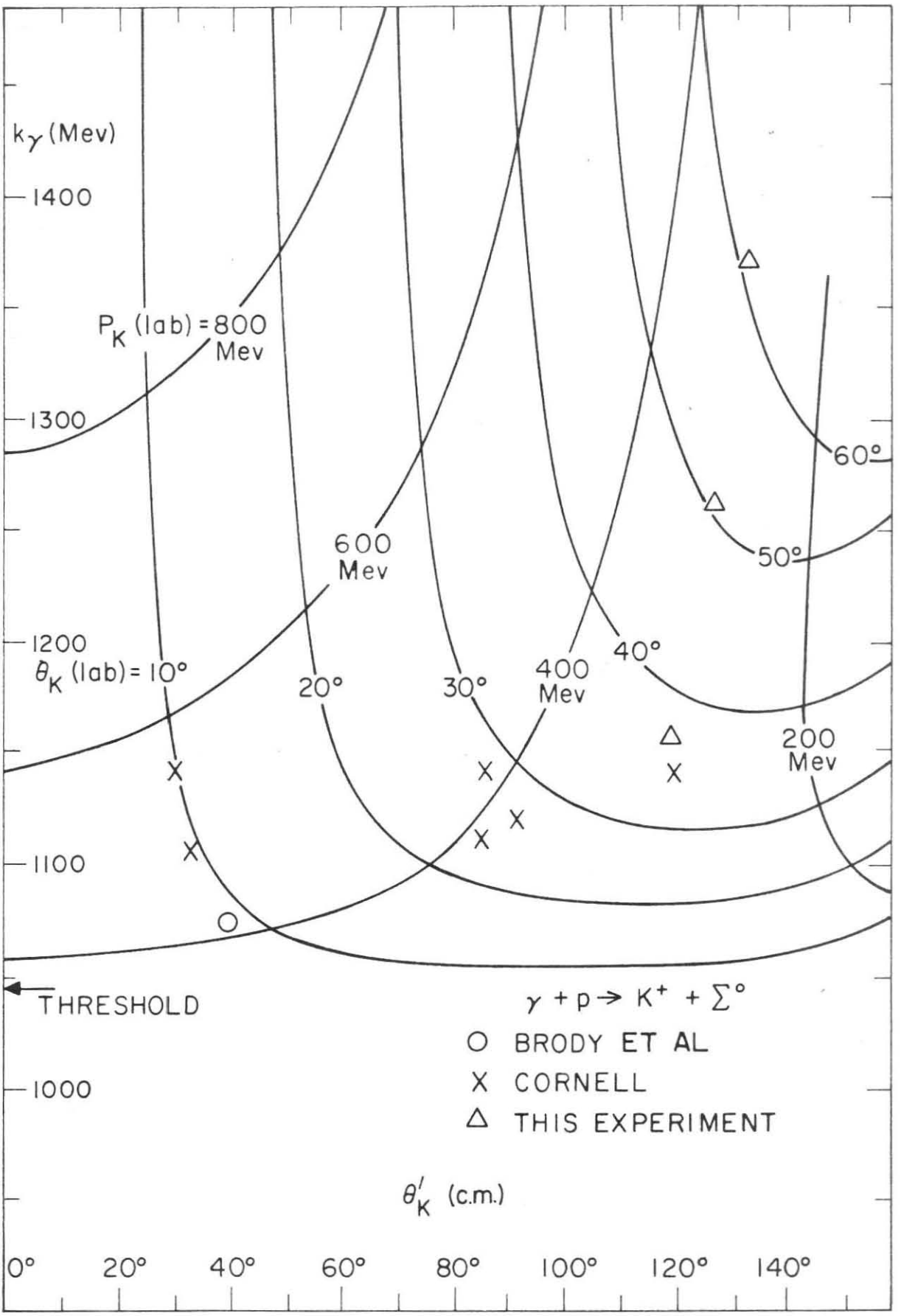
k_γ (Mev)
1400
1300
1200
1100
1000
P_K (lab) = 800 Mev
600 Mev
400 Mev
200 Mev
θ_K (lab) = 10°
20°
30°
40°
50°
60°
THRESHOLD
$\gamma + p \rightarrow K^+ + \Sigma^\circ$
O BRODY ET AL
X CORNELL
△ THIS EXPERIMENT
θ'_K (c.m.)
0° 20° 40° 60° 80° 100° 120° 140°

II. EXPERIMENTAL METHOD

A. General

The experiment was performed by detecting the meson produced in one or the other of the reactions:

$$\text{a)} \quad \gamma + p \rightarrow K^+ + \Lambda^\circ$$

$$\text{b)} \quad \gamma + p \rightarrow K^+ + \Sigma^\circ$$

using a magnetic spectrometer to measure the momentum and angle of the meson after it emerged from a proton (hydrogen) target placed in a γ -ray beam. Given this momentum and angle, along with the identity of the particles involved in the reaction, one may determine the kinematical properties of all of the members of the interacting system, including the incoming gamma ray. This follows from the conservation of energy and momentum, and the fact that we are dealing with the interaction of only two particles. It is necessary to use the kinematics to find the energy of the γ -ray initiating reaction a) or b) above, since the beam of an electron synchrotron contains photons of all energies between zero and the peak energy attained by the electrons in the machine.

Since the threshold for reaction b) is about 135 mev above that for reaction a), it is in general possible (with sufficient resolution) to run the synchrotron in such a way as to emit no photons with enough energy to produce a K meson from reaction b) capable of reaching the detector. By using this technique, reaction a)

may be studied without interference from reaction b). If the peak energy of the γ-ray spectrum is then increased, the rates for a) and b) combined can be measured. Information about reaction b) can then be obtained by subtracting the contribution from a). The second process is thus considerably more difficult to study than the first, since enough counts must be accumulated at each energy to make the difference of the two counting rates statistically meaningful.

Another way to separate the two types of event would be to determine the identity of the hyperon produced. Under the conditions of the present experiment, this was impractical for several reasons. First, the Λ°'s were emitted at about 15° to the incoming γ-ray beam, and the Σ°'s came out at an even smaller angle, around 13°. The Σ° decays essentially instantaneously by

$$\Sigma^\circ \rightarrow \Lambda^\circ + \gamma$$

producing a 74 mev γ-ray. The decay Λ° makes an angle of less than 4° to the initial Σ°, and therefore, except for having about 90 mev (20%) more energy in the laboratory, looks very much like the Λ° from $\gamma + p \rightarrow \Lambda^\circ + K^+$. The only practical method for detecting Λ°'s in this type of experiment is by detecting one or the other of its decay products,

1) $\Lambda^\circ \rightarrow p + \pi^+$ 60%

2) $\Lambda^\circ \rightarrow n + \pi^\circ$ 40%
$\quad\quad\quad\quad\quad\quad\quad\quad\quad\quad\quad\quad \llcorner 2\gamma$

These decays take place within three or four centimeters of the place where the Λ° is produced. The decay nucleon in both cases stays within 9° of the initial Λ° direction, and is close enough to the direction of the synchrotron photon beam to be completely impractical to detect. The decay pion, on the other hand, is emitted at a laboratory angle as large as 45° to the initial Λ°. Detecting this pion efficiently and determining its kinematic properties well enough to detect a difference of 90 mev in the energy of the original Λ° is fairly difficult. This is especially true as the π° would have to be detected by means of its decay into two γ-rays.

The other possible way of distinguishing the $\gamma + p \rightarrow K^+ + \Sigma^\circ$ process is by looking for the γ-ray from the decay of the Σ°. However, since less than half of these γ-rays come forward of 45° in the laboratory (with respect to the decaying Σ°) the method is inefficient, and even if the inefficiency could be tolerated, the γ-ray background from other sources, especially 2) above, would be appreciable.

The main features of the method used for detecting K mesons are shown in figure 3. The collimated bremsstrahlung beam from the Caltech synchrotron passed through the hydrogen target and on to the beam monitor. Those K^+ mesons having the proper angle and momentum passed out through the target walls and were focused by the spectrometer magnet onto a counter telescope in which they were stopped by their ionization losses. These

ionization losses were measured by the counters, and helped to determine the velocity of the mesons.

FIGURE 3

THE EXPERIMENTAL METHOD

The dark rectangles are absorbers.

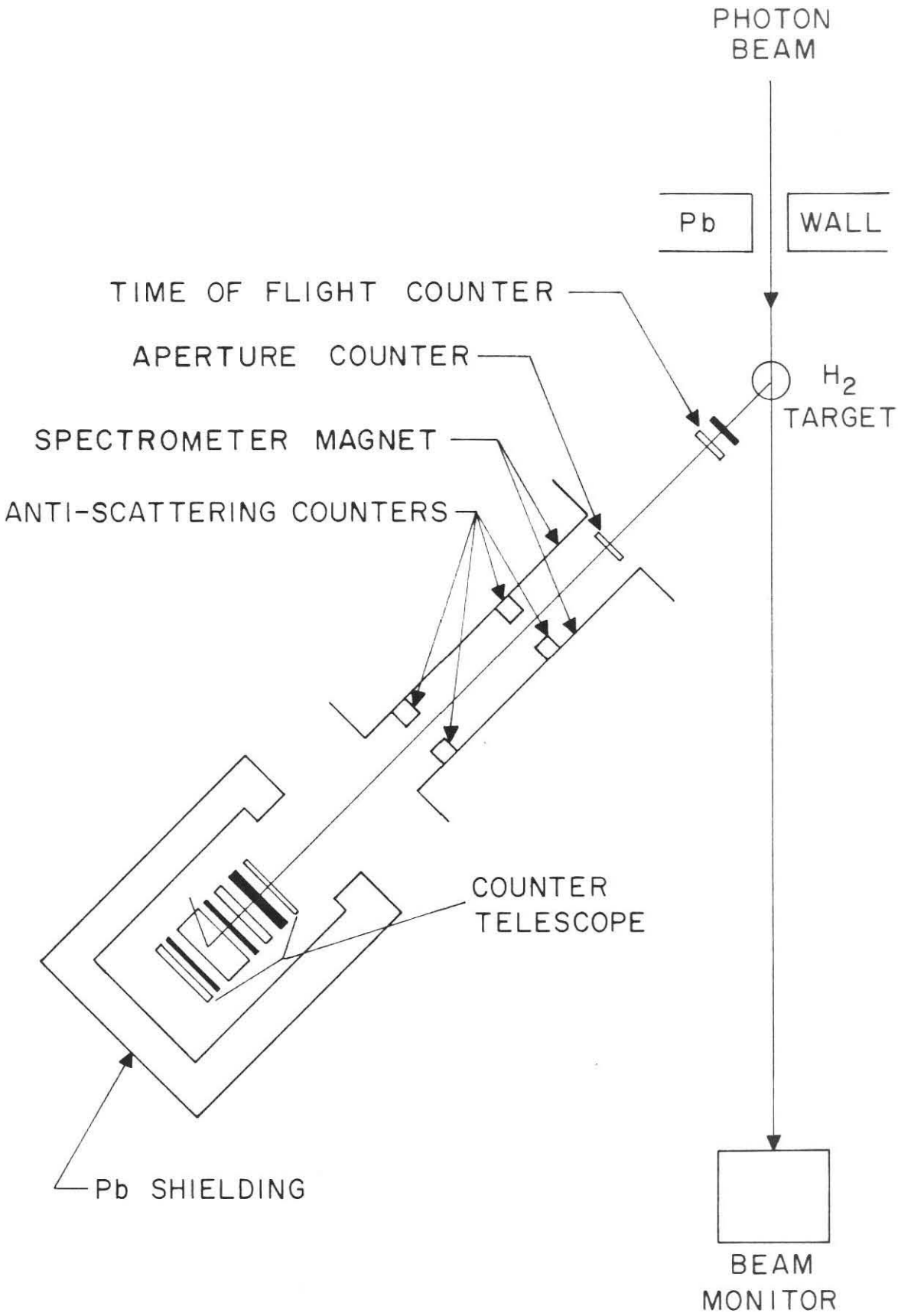
PHOTON
BEAM
Pb
WALL
TIME OF FLIGHT COUNTER
APERTURE COUNTER
H_2
TARGET
SPECTROMETER MAGNET
ANTI-SCATTERING COUNTERS
COUNTER
TELESCOPE
Pb SHIELDING
BEAM
MONITOR

Another velocity check was made by measuring each meson's flight time over the path from the time of flight counter, near the target, to the counter telescope. With the velocity given by the ionization and time of flight measurements, and the momentum fixed by the spectrometer, it was possible to determine each particle's mass, and hence its identity. Such an extensive detection system was necessary in order to reduce the background of about 2000 pions and "unlikely" proton events present for each K meson detected to an acceptable level without throwing out many K mesons, since K counting rates were less than 5 per hour.

B. Apparatus

1. Photon Beam.

A plan view of the experimental area as it was during the running of this experiment is shown in figure 4. The photon beam emerges from the synchrotron, is collimated by the collimator, and then passes through a thin ion chamber and a lead scraper. Photons and electrons scattered by the collimator are removed from the region around the beam line by this scraper. Beyond the scraper, the beam passes through targets used in other experiments and is then "swept" by a "broom" magnet which straddles the beam. The collimator, as well as these targets, generate charged particles, which this magnet bends out of the beam line so that they may be removed by the second scraper. Three feet past the second

FIGURE 4

PLAN VIEW OF EXPERIMENTAL AREA

Caltech 1500 mev electron synchrotron at upper right.

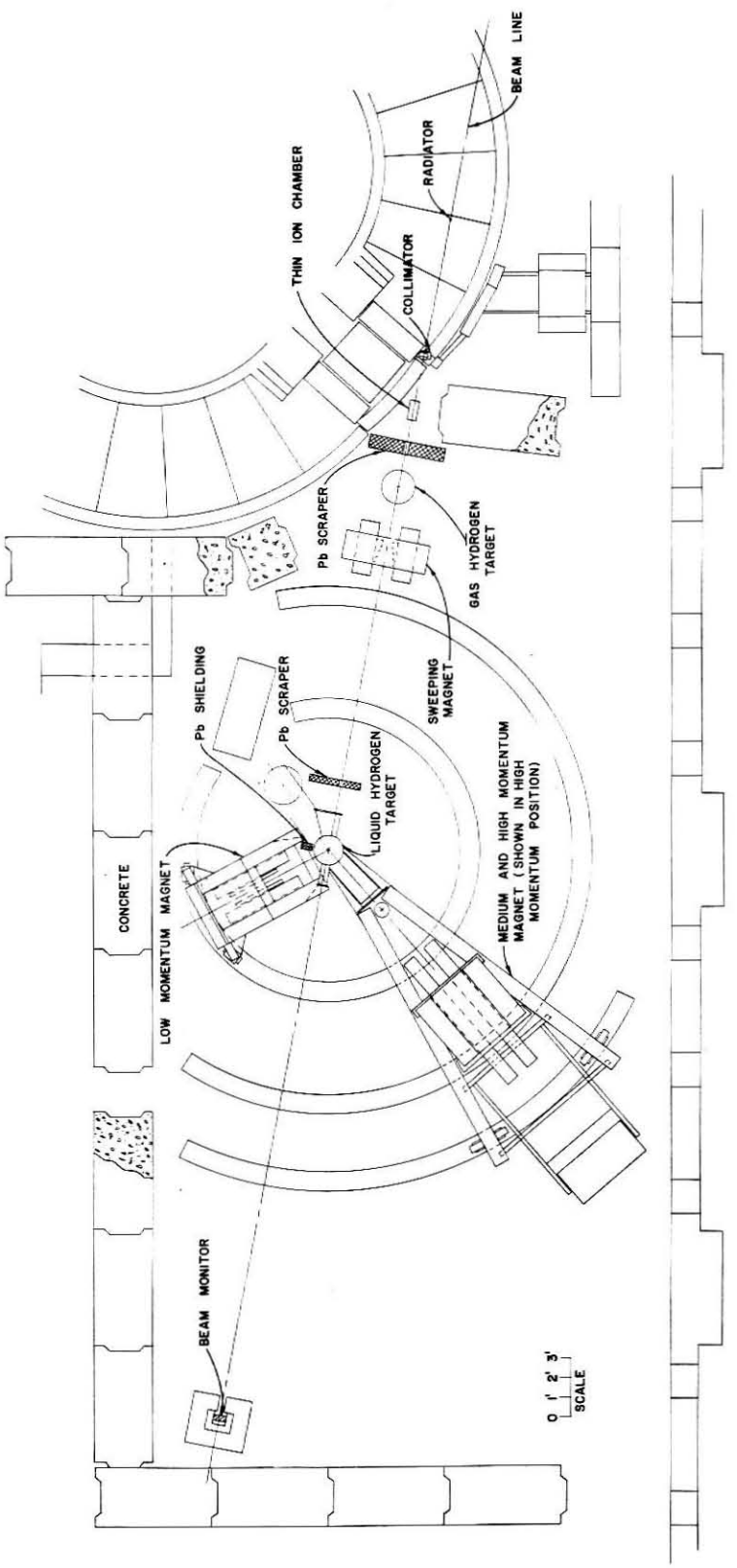
BEAM LINE
RADIATOR
THIN ION CHAMBER
COLLIMATOR
Pb SCRAPER
GAS HYDROGEN TARGET
SWEEPING MAGNET
Pb SHIELDING
Pb SCRAPER
LIQUID HYDROGEN TARGET
CONCRETE
LOW MOMENTUM MAGNET
MEDIUM AND HIGH MOMENTUM MAGNET (SHOWN IN HIGH MOMENTUM POSITION)
BEAM MONITOR
0 1' 2' 3'
SCALE

scraper the γ -ray beam enters the liquid hydrogen target used in the present experiment and then continues on to the beam monitor, where it is absorbed.

The spectrum of the bremstrahlung beam has been measured by Donoho, Emery, and Walker (11), and, more recently, by Boyden and Walker (12). Their measurements are described in terms of a spectrum function, $B(E_o, k/E_o)$, defined by:

$$n(k)\ dk = \frac{W}{E_o} B(E_o, k/E_o) \frac{dk}{k} ,$$

where $n(k)\ dk$ is the number of photons in the interval k to $k + dk$ for a beam of total energy W and peak photon energy E_o. The function $B(E_o, k/E_o)$ has the useful properties that it is

a) almost independent of E_o,

b) only slightly dependent on k/E_o for k/E_o between about 0.5 and 0.95, in the range of E_o of this experiment, and

c) normalized such that $\int_0^1 B(E_o, k/E_o)\, d(k/E_o) = 1$.

To find $n(k)\ dk$, it is necessary to know W and E_o as well as $B(E_o, k/E_o)$. The total energy in the beam, W, is monitored by the thick copper ionization chamber in which the photon beam is finally absorbed. The total current flowing from the ionization chamber during a run is integrated by a precision integrator which resets itself and advances a register every time it accumulates

a certain amount of charge. This amount of charge (and hence of total beam energy, which is proportional to the charge) defines a unit known as the BIP (for Beam Integrator Pulse). A special precision charge source was developed to determine accurately the number of coulombs per BIP. This number was measured frequently during the experiment, and found to be constant at 0.2109×10^{-6} coulombs per BIP within $\pm$ 0.2 %.

The absolute calibration of the ion chamber was done by R. Gomez (13) using a "Cornell" type quantameter (14). This calibration depends somewhat on E_o, and also very slightly on time, due to a slow gas leak. At 0° C and 760 mm Hg, the absolute calibration of the chamber used is $3.933 \left[1 + 0.0630 \ (1 - E_o) \right] \times 10^{18}$ mev/coulomb, where E_o is the peak photon energy in bev.

During part of the experiment, the photon beam was stopped by another magnet in the beam downstream from the liquid hydrogen target. For these runs, the beam was monitored by a thin ionization chamber near the collimator, as the main ionization chamber was partially eclipsed by this other magnet. This thin chamber was calibrated against the main chamber every hour or two, and all counting rates were reduced to rates per main beam monitor BIP.

At the 1383 mev Σ° point, a portion of the electron beam in the synchrotron spiralled into the radiator before reaching

full energy. This caused about 10% to 30% of the photon beam to spill out of the machine with poorly defined peak energy; any effect on the experiments in progress was eliminated by gating off all detectors and the beam energy integrator until the internal electron beam had reached full energy. The error introduced by this gate was estimated to be less than 1%.

The remaining factor in $n(k)\,dk$, E_o, is determined by measuring accurately the magnetic field of the synchrotron at the time the electron beam strikes the radiator. Knowing this and the radius of curvature of the electron orbit, it is possible to calculate E_o quite accurately.

2. The Hydrogen Target. The target is a cylindrical Mylar cup 3" in diameter filled with liquid hydrogen. The cup is surrounded by an evacuated region containing heat shields cooled by liquid nitrogen. The outer wall of the vacuum chamber is a 16" diameter cylinder concentric with the target cup, with tubes projecting from it in both directions along the photon beam line (figures 4 and 5). The beam enters and leaves the vacuum chamber through Mylar windows at the ends of these tubes. These beam windows are far enough from the target cup that they are not seen by the spectrometer system, and hence a potential source of background is eliminated. This target is basically the one designed by V. Z. Peterson and used by Donoho and Walker (2), and Brody, Wetherell, and Walker (5), but has since been modified by Walker to reduce background originating in the target structure itself.

FIGURE 5

THE MAGNETIC SPECTROMETER AND COUNTER TELESCOPE

The momentum dispersion of the spectrometer, $\frac{\Delta p_o}{p_o}$, is 0.081 and its nominal solid angle is 0.0194 steradian. The path length between foci is 94.8 inches.

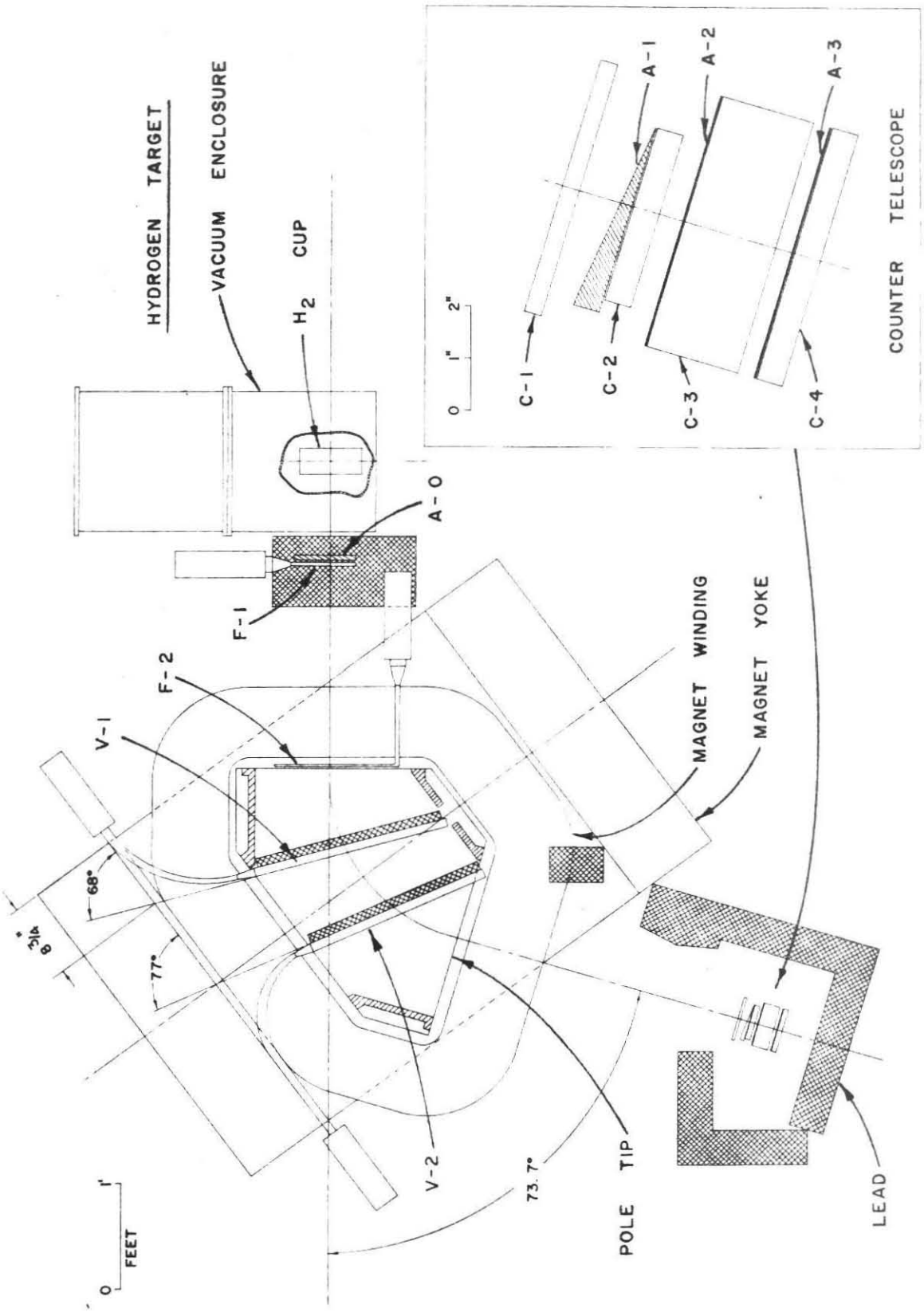
HYDROGEN TARGET
VACUUM ENCLOSURE
H_2 CUP
A-0
F-1
F-2
V-1
V-2
68°
77°
θlab
0
1'
FEET
73.7°
POLE TIP
MAGNET WINDING
MAGNET YOKE
LEAD
COUNTER TELESCOPE
A-1
A-2
A-3
C-1
C-2
C-3
C-4
0
1"
2"

3. Magnetic Spectrometer. The magnet used to focus particles from the target onto the counter telescope was the "Low Momentum Magnet" designed by Vette (15). It is a single focusing magnet producing a (nearly) uniform field over a wedge-shaped region (figure 5).

The whole magnet-counter assembly pivots about a vertical axis through the hydrogen target, so that it is quite easy to vary the emission angle, θ_{lab}, of the particles accepted by the spectrometer. The magnetic field (and therefore the momentum of the particles detected) may be held constant to within one part in 10^4 by regulating the current through the magnet windings. This field was monitored with a proton resonance magnetometer (15), and remained constant to within $\pm$ 0.1% throughout the experiment. At 15.00 Kg., close to the maximum field, the central momentum through the magnet is 273.0 mev/c.

In order to detect particles with momentum greater than that for which the spectrometer was set that might traverse the path from the target to the counter telescope by scattering from the magnet pole tips, the pole tips were lined with anti-scattering ("fan") counters. These counters were long narrow strips of scintillation plastic which, in conjunction with the "aperture counter" to be described later, made it possible to eliminate these scattered particles. This was accomplished by requiring that an acceptable

event pass through the aperture counter and into the telescope without passing through a fan counter. The rear pair of counters (V-2) also served to define the solid angle of the system in the horizontal direction. Thin lead absorbers were placed in front of each fan counter to reduce its singles counting rate. Long lucite light pipes carried the light output from the scintillators to a pair of 6810 photomultipliers. By locating these photomultipliers outside the magnet yoke, it was much easier to shield them from magnetic field effects.

The aperture counter F-2 had three functions: first, it defined the vertical limits of the solid angle of the detection system; second, since it was in fast coincidence with the counter telescope, it reduced accidental counts; and third, it formed part of the anti-scattering system mentioned above. As shown in figure 5, this counter was placed just outside the front edge of the magnet pole tips. Being this far into the fringe of the magnetic field, F-2 was well protected from flooding by low energy charged particles. In F-2, light coming down from the scintillator was reflected by a mirror through 90 degrees into a light pipe leading to a photomultiplier outside the magnet yoke. This somewhat unorthodox arrangement was used to get the photomultiplier on the bottom end of the counter. This way, the finite transit time of the light down the length of the

counter tended to compensate, rather than augment, fluctuations in the time of flight measurements introduced by the variations in the lengths of the flight paths through the magnet.

4. Counter Telescope. A group of four scintillation counters separated by absorbers was mounted in a lead cave at the rear focus of the magnet (figure 5). All four counters were made by coupling one end of a rectangular slab of plastic scintillator to a single RCA 6810 photomultiplier by means of a Lucite light pipe about 6" long.* For better light gathering efficiency, a front surfaced mirror was fastened directly against the other end of the slab with silicone grease and the whole scintillator--light pipe assembly was then wrapped in bright aluminum foil. Not only the counters in the telescope, but also each of the other counters in the experiment was assembled in this way. Every photomultiplier used was shielded electrostatically and magnetically in the following manner: first the glass envelope of the tube, except for the photo-cathode, was wrapped in an aluminum foil layer which was maintained at cathode potential; outside of this was a layer of cellulose acetate insulation, and then a layer of Fernetic-Conetic** magnetic shielding; and finally, the whole assembly was enclosed in a soft iron cylinder.

---

* The theory of these light pipes has been discussed by Garwin (16).

** Manufactured by Perfection Mica Company, 1322 Elston Ave., Chicago, Illinois.

The dimensions of all counters used are given in Table I. The properties of the various absorbers are listed in Table II.

The telescope was designed in such a way that a K meson of the momentum accepted by the spectrometer makes a signal proportional to its specific ionization loss in both C-1 and C-2 and then stops in the back half of C-3. Counter C-2 also serves to define the momentum acceptance and dispersion of the magnet system. Pions of the proper momentum to pass through the system have a range more than four times the thickness of the counter telescope and therefore could be strongly discriminated against by placing a fourth counter C-4 in veto with C-1, C-2, and C-3. Some pions were absorbed before C-4, and these had to be thrown out by other means. The energy of the protons accepted by the magnet is so much lower than that of the K mesons that they came to rest before penetrating C-2. The only protons detected by the telescope, then, are those with the wrong momentum which manage to get by the anti-scattering system without enough range to reach C-4. It would have been useful to have been able to place a Cerenkov counter somewhere ahead of C-3 to veto pions before they had a chance to interact but the range of the K mesons is so small that a counter thick enough to produce a useful Cerenkov signal was not practical. In addition to this objection, the Cerenkov counter would not have been

TABLE I

Description of Scintillation Counters

Counter	Dimensions (inches)	Thickness (gm/cm^2)
F-1	3-1/4 x 6-1/2 x 3/8	1.00
F-2	3 x 13 x 1/4	0.67
V-1	1/2 x 20-3/4 x 1-13/16	
V-2	(3/4 to 13/32) x 21 x 15/16	Uniformly tapered
C-1	5-3/16 x 8-1/2 x 1/4	0.667
C-2	3-25/32 x 8-1/4 x 13/32	1.08
C-3	5-1/2 x 8-1/2 x 1.70	4.56
C-4	5-1/2 x 8-13/32 x 1/2	1.47

Note: All photomultipliers are RCA 6810 A

TABLE II

Description of Absorbers

Absorber	Material	Thickness (inches)	gm/gm^2
A-0	Lucite	0.500	1.11
A-1	Lucite	0.025 to 0.465	0.067 to 1.232
A-2	Copper	0.021	0.477
A-3	Copper	0.021	0.477

Note: A-1 is a uniform wedge

able to detect pions interacting early in the counter telescope and producing slow charged secondaries. This latter type of event was presumably the most important type of pion background.

Because of the short range of the K mesons detected, a minimum of absorber was used between the counters. No absorber was used in front of C-1 in order to minimize the number of pion interaction events that occurred before any ionization measurements could be made on them. The absorber between C-1 and C-2 was built in the form of a wedge so that the particles traversing the thick end of the wedge, whose average momentum was higher than the momentum of those going through the thin end, would be slowed down more. This method of narrowing the velocity spread of the particles helped to make the pulse spectra from C-2 and C-3 narrower.

Thin copper plates (A-2 and A-3) were placed between C-2 and C-3 and between C-3 and C-4 to isolate the counters from each other and to prevent delta rays produced in one counter from entering another. Also, A-3 prevented the lower energy decay products from K mesons stopping in C-3 from reaching C-4 and vetoing K events.

The whole telescope was surrounded by four inches of lead except for a rectangular opening at the top. More lead was stacked inside the magnet yoke to prevent any of the rear counters from seeing the hydrogen target directly.

5. Time of Flight System. The system for measuring flight times of particles through the spectrometer consisted of F-1, C-3 (figure 5), and a specially developed "chronotron" connected between them by means of a pair of coaxial cables. (An absorber A-0 was placed in front of F-1 to reduce counts due to low energy background from the hydrogen target.) A particle would trigger F-1 at time t_o, and arrive at C-3 at a later time, t. By making the length of the cable to F-1 longer than that to C-3, it was possible to delay the signal from F-1 long enough that it arrived at the chronotron at about the same time as the signal from C-3. If a faster particle went through F-1 at time t_o, the pulse it produced in C-3 would arrive at the chronotron before the pulse from F-1, and so on. In order to separate the K mesons from the pions, the chronotron had to be able to measure these time differences well enough to detect flight time variations of less than 3 nanoseconds (3×10^{-9} seconds). It was also highly desirable that its time-measuring properties be stable over long periods of time. Such a device will now be described.

At the top of figure 6, two pulses direct from the anodes of their respective phototubes are shown arriving at the inputs of the chronotron, slightly displaced in time. Their height and width are standardized by the shapers S and each one continues down its own 6 nanosecond long piece of coaxial cable. At the end of the cable,

each pulse is absorbed in the termination. Fast diode coincidence circuits C connect three pairs of points along the cables, as shown. The response of one of these diode circuits is shown in figure 7a. Each diode circuit sees a different time separation of the incoming pulses because of the extra 6 nanosecond delay introduced by the cables (see figure 7b). For example, as shown in figure 6, if the right hand pulse arrives at S first, the signals out of the three "C's" will appear as shown. Some possible sets of inputs and outputs are given at the bottom of the figure. In order to display the three pulses from the C's on an oscilloscope, they are split by the duplexers M and then delayed about 150 nanoseconds with respect to one another and mixed. The other signal from each duplexer may be fed into an adder without being delayed first. The response function of the "sum output" of this adder for two different sets of input pulses to the adder is shown in figures 7c and 7d. Any pulse from this output whose height is greater than the discriminator bias (dotted line) will trigger the discriminator on the input to the slow coincidence circuit (see section B-6 and figure 9). This sum output is used as a broad (20 nanosecond resolving time) coincidence to indicate when a particle passes through the system with flight time close enough to that of a K meson to warrant taking an oscilloscope picture of the triplet output of the chronotron. Samples of this triplet output may be seen in figure 14, labeled "Ch II".

FIGURE 6

OPERATION OF THE CHRONOTRON

At the bottom of the figure are shown the output pulse trains for various time separations of the input pulses. "T" is the time parameter discussed in the text.

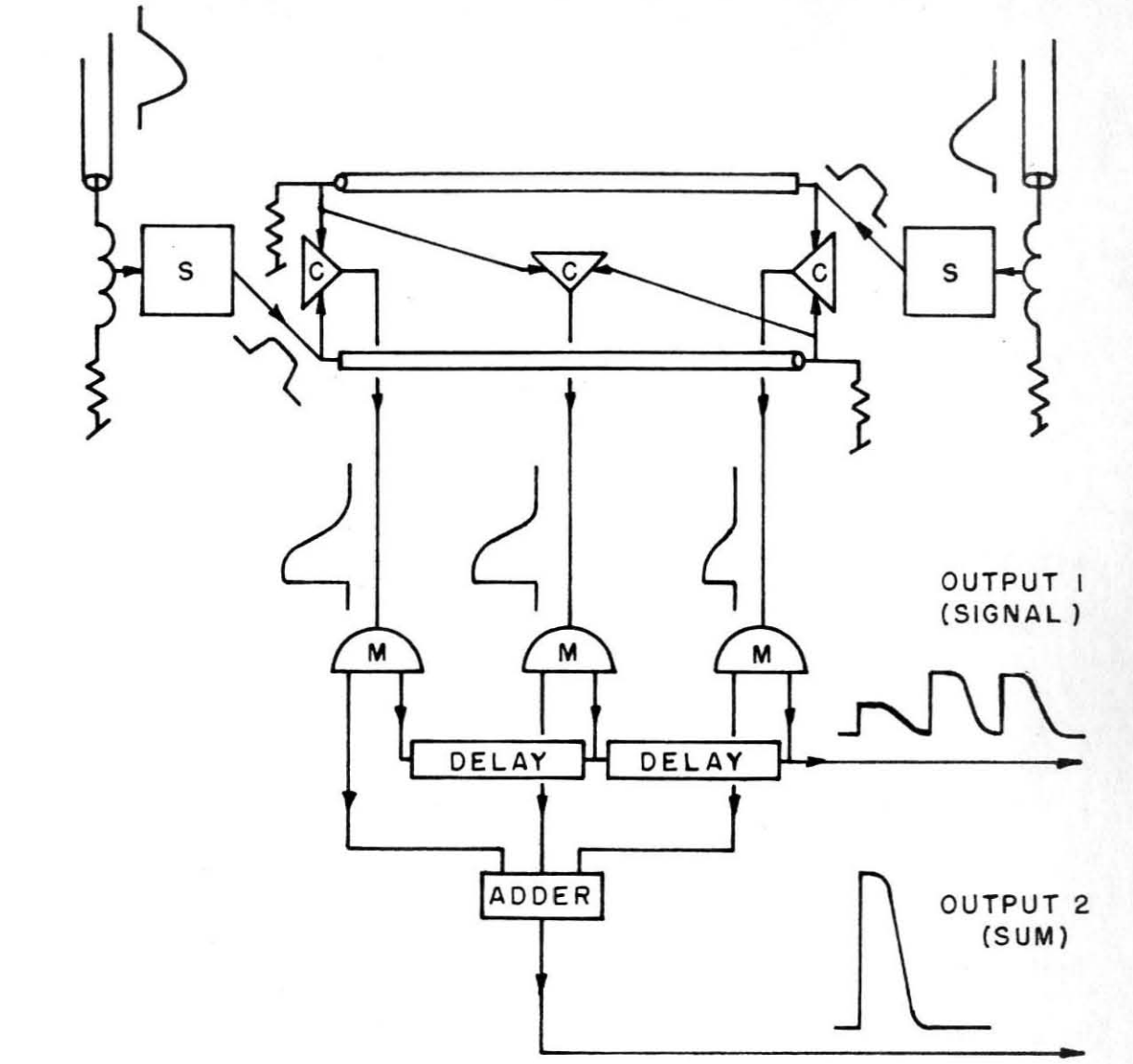
S
C
C
C
S
M
M
M
DELAY
DELAY
ADDER
OUTPUT 1
(SIGNAL)
OUTPUT 2
(SUM)

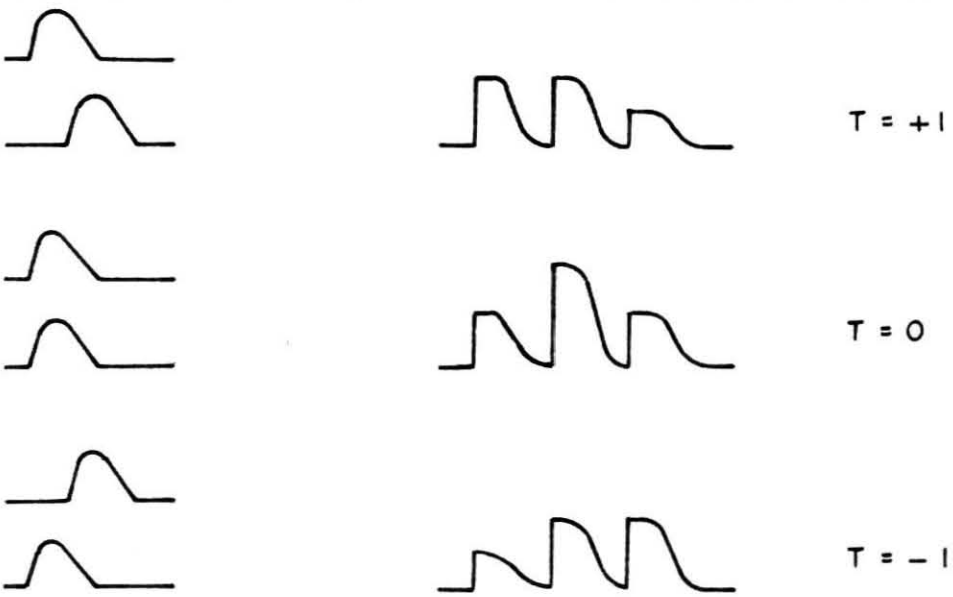
T = +1
T = 0
T = −1

FIGURE 7

CHRONOTRON RESPONSE FUNCTIONS

All four diagrams are drawn to the same time scale.

a) Idealized response of a single diode coincidence ("C", figure 6). Output pulse height is shown as a function of the time interval between input pulses.

b) Response of each of the three single coincidences, showing relative displacement principle on which the chronotron is based.

c) Response of the "sum output" of the chronotron, formed by combining the three curves of part b) above.

d) Response of the "sum output" when only the center and right hand single coincidences are combined by the adder. Dotted lines here and in figure 6c) above show the effect of the discriminator. It is seen that the effect of combining only this pair of the three single coincidences is to discriminate against negative values of Δt .

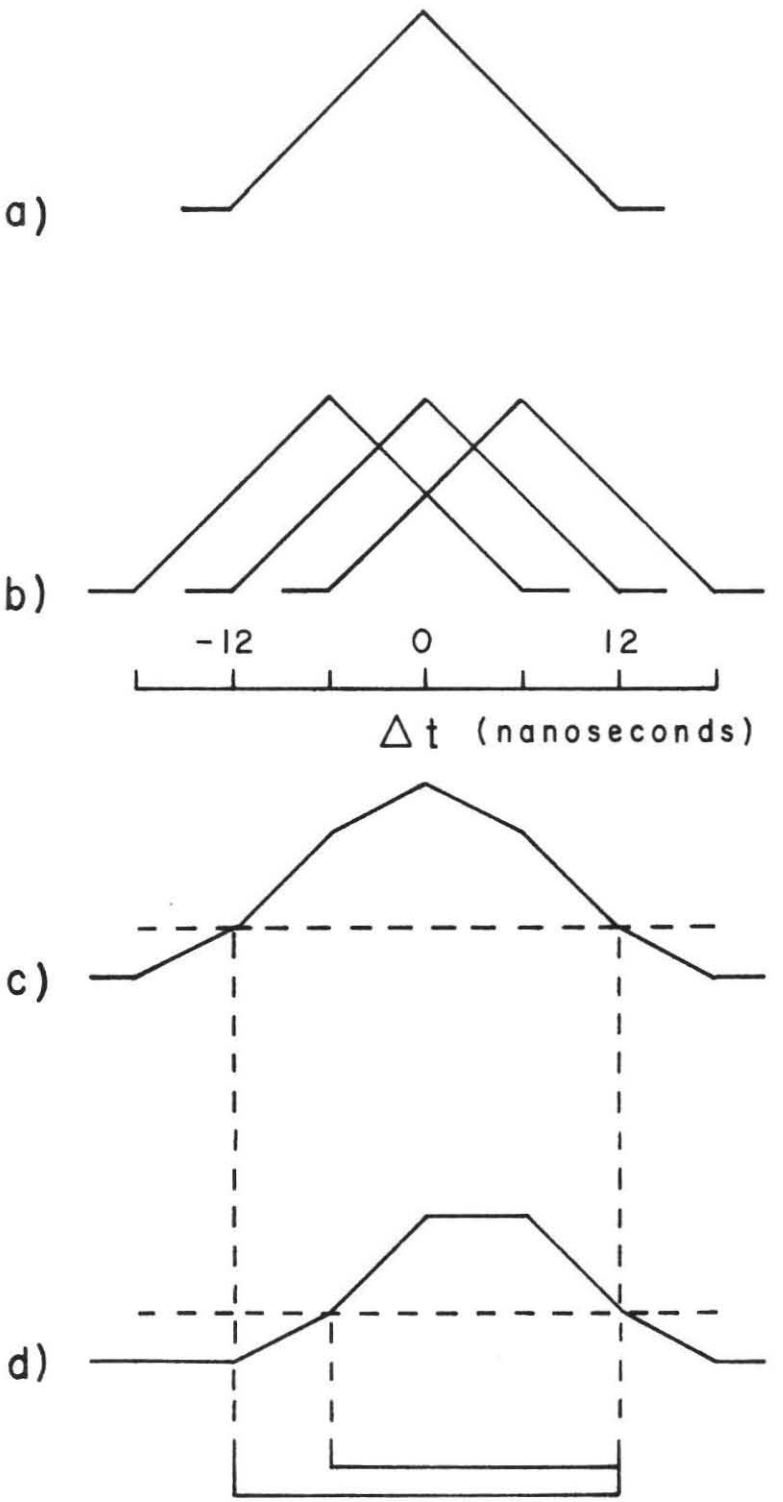
a)
b)
-12
0
12
Δ t (nanoseconds)
c)
d)

Although slightly more complex than an ordinary coincidence circuit, the chronotron had several things to recommend it. The most important of these was its ability to measure small time differences accurately over a range about three times as large as that of a single coincidence circuit. Because of this feature, it was possible to obtain actual time of flight spectra, with both K meson and pi meson peaks visible in one set of runs. It was thus possible to see the separation between the two types of event (figure 16). Also, the K meson time of flight peak had a natural spread of about 4 nanoseconds, and it was helpful to be able to set this peak safely inside the wide sensitive region of the chronotron.

The three pulse heights from the chronotron's output were inconvenient to use directly in analyzing the data, so a single parameter characterizing the triplet, and closely related to the time difference between arriving signals, was sought. Such a parameter, T, was found, and is given by:

$$T = 10 \left[\frac{(1) - (3)}{(2) - \min(1,3)} \right]$$

where (1) is the height of the first pulse in the triplet, (2) is that of the second, and so on, and min (1, 3) is the height of the smaller of (1) and (3).

By delaying one of the inputs to the chronotron by varying amounts it is possible to measure T as a function of the time

separation of the two input pulses at the chronotron. A series of such measurements was made using the actual time of flight signals from pions, along with a switchable delay box having one nanosecond steps. About fifty pion signals were recorded for each delay, and the average value of T, $\overline{T}$, was plotted versus delay (figure 8). It is seen that T is quite linear over a range of at least ± 10 nanoseconds from exact coincidence. The slope of the line is 2.74 ± 0.06 per nanosecond. Besides being linear, this parameter has the great advantage of depending only on the ratio of the pulse heights in the triplet. For this reason, T is independent of changes in the gain of any of the electronics beyond the duplexers M mentioned above.

The only three places where drifts affecting T can occur, other than in the photomultipliers, is in the shapers, the diode coincidences, or the duplexers. Stabilized d.c. supplies are used for all three components, and the vacuum tube filaments in the shapers and the duplexers are fed by a regulated a.c. supply. Shaping is done by having the (negative) input pulse turn off a pentode (E180F) carrying a definite plate current, then clipping the plate signal with a shorted stub. Thus the only part of the shaper circuit subject to drift is the d.c. plate current in the pentode. A metering system is built into the chronotron so that these plate currents can be monitored easily, and adjusted when necessary. The average time of flight as measured by this system remained constant within ± 0.3 nanoseconds (all of which

FIGURE 8

TIME PARAMETER, T, VERSUS DELAY

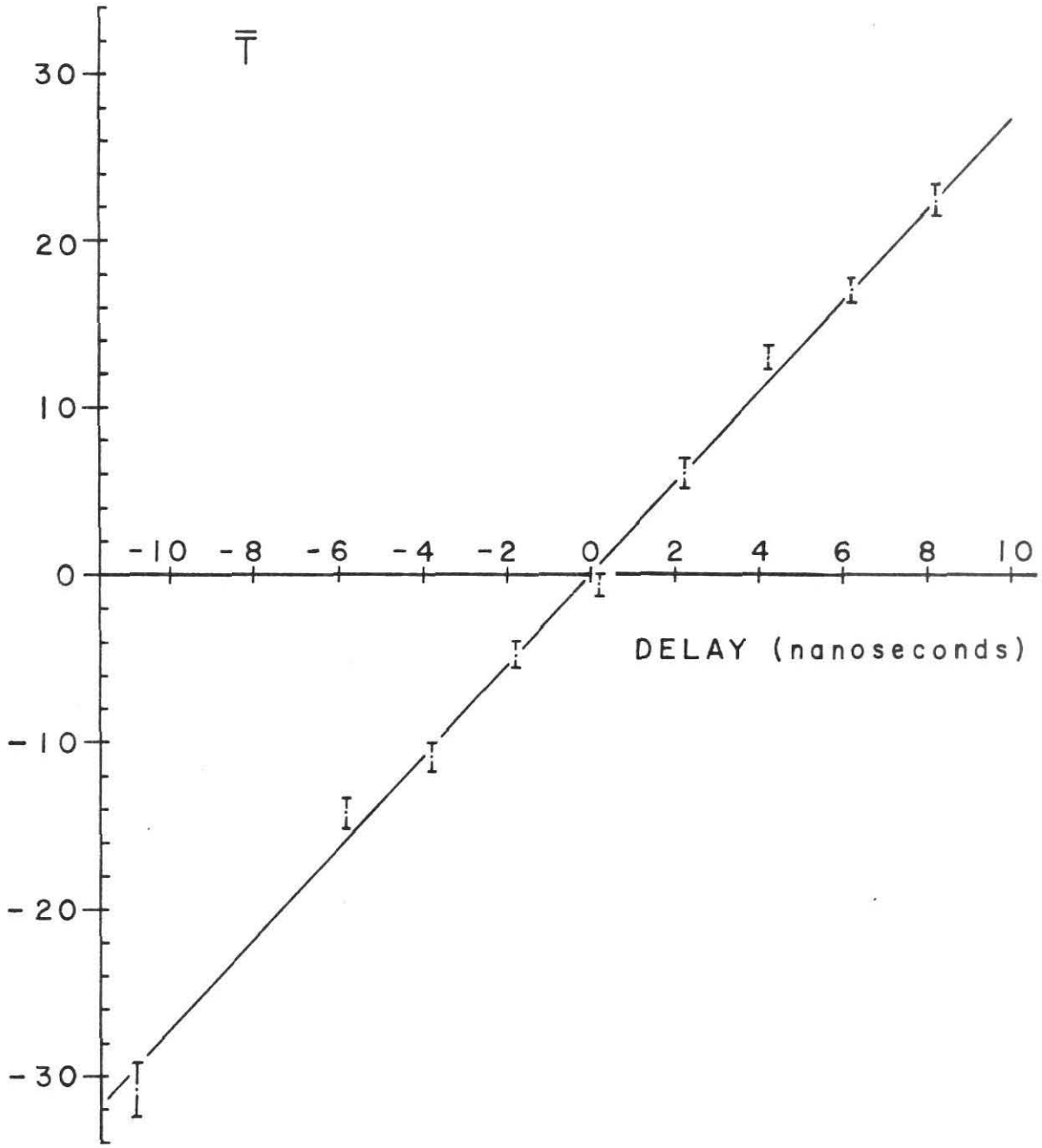
$\overline{T}$
30
20
10
0
-10
-20
-30
-10
-8
-6
-4
-2
0
2
4
6
8
10
DELAY (nanoseconds)

may be accounted for by statistical fluctuations) for the entire period of several months required for this experiment.

The time resolution of the chronotron itself was measured by measuring the flight time of pions between two scintillation counters placed three inches apart at the focus of the magnet. Any fluctuations in the flight time could be ascribed to effects produced by jitter in the shape and height of the pulses from the photomultiplier, due mostly to spread in the ionization losses of the pions in passing through the scintillators. The resolution of the counters used was about 30 % full width at half maximum. To avoid errors that might be introduced by the fact that light itself takes a finite time to travel down the length of a counter, both scintillators were placed normal to the pion beam during these tests, and viewed from the side by photomultipliers placed on the same side of the beam. These measurements showed that T was approximately Gaussian, with a standard deviation of 0.7 nanoseconds.

6. Electronics. A diagram of the electronics used to amplify, select, and display information from the various counters and coincidence circuits is shown in figure 9. Signals from the tenth dynodes of C-1, C-2, and C-4, and from the twelfth dynode of C-3 are stretched to about 400 nanoseconds in the preamplifier. The C-1, C-2, and C-3 pulses are then amplified, delayed, and mixed with the veto pulse (if any) from the fan coincidence circuit. These four pulses, along with that from C-4, then enter the "low level mixer", so-called

FIGURE 9

ELECTRONICS BLOCK DIAGRAM

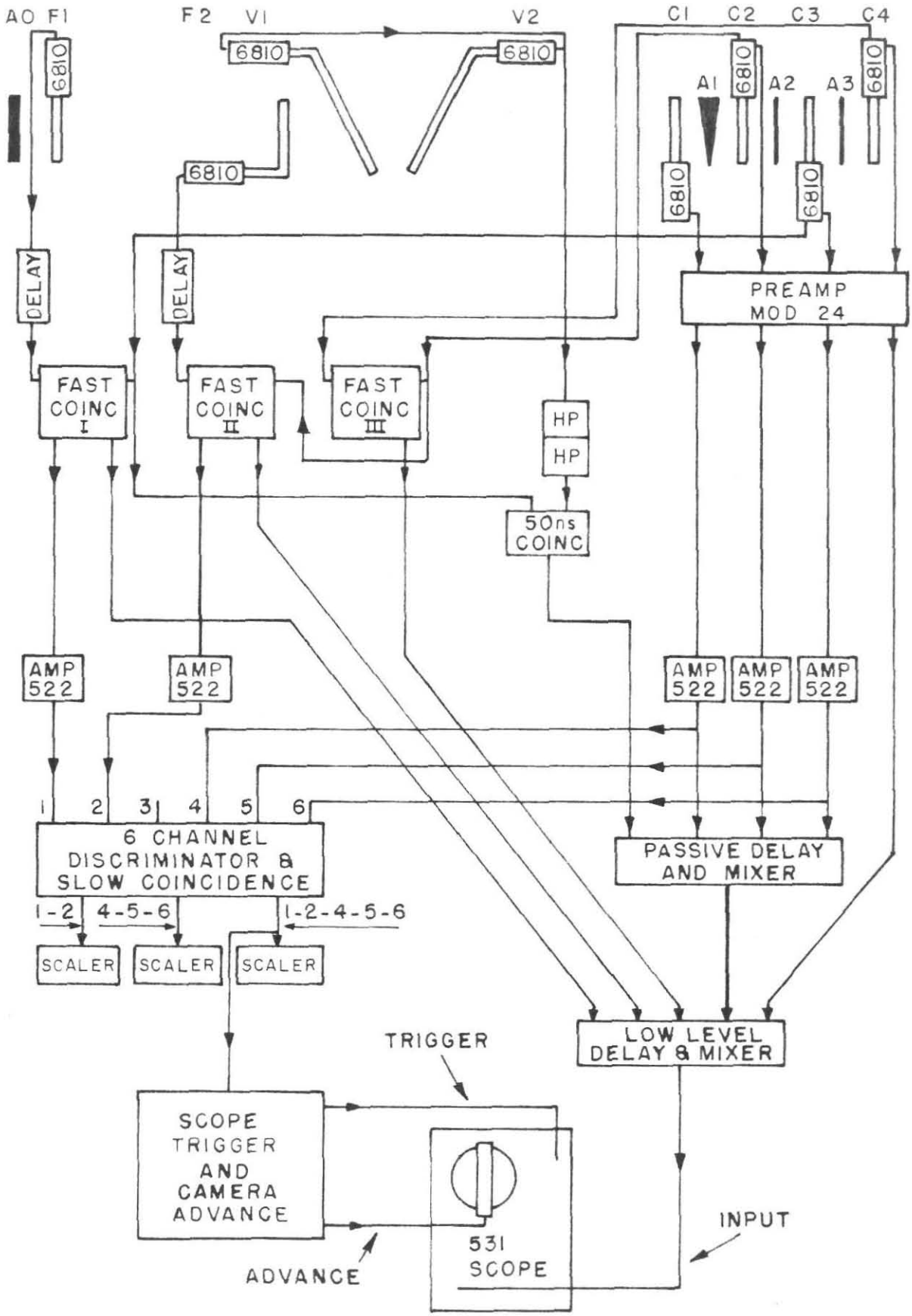
A0 F1
F2 V1
V2
C1 C2 C3 C4
A1 A2 A3
6810
DELAY
PREAMP MOD 24
FAST COINC I
FAST COINC II
FAST COINC III
HP
HP
50ns COINC
AMP 522
1 2 3 4 5 6
6 CHANNEL DISCRIMINATOR & SLOW COINCIDENCE
PASSIVE DELAY AND MIXER
1-2
4-5-6
1-2-4-5-6
SCALER
LOW LEVEL DELAY & MIXER
TRIGGER
SCOPE TRIGGER AND CAMERA ADVANCE
ADVANCE
531 SCOPE
INPUT

because it contains active elements and does not attenuate the low level input signal. It is necessary to amplify the outputs of C-1, C-2, and C-3, since the six-channel gated discriminator described below requires large input pulses.

The triplet output of the chronotron (labelled "fast coinc I") described above, as well as that of each of the other similar fast coincidence circuits shown are also fed into the low level delay-mixer. "Fast coinc II" connects C-2 in the counter telescope with F-2, the aperture counter, and "fast coinc III" was used between C-3 and C-4 in an unsuccessful attempt to distinguish pions passing through the telescope from K mesons whose decay products passed through C-4.

The "sum outputs" of I and II, as well as the amplified outputs of C-1, C-2, and C-3 are fed into a discriminator and slow coincidence circuit with a resolving time of about 200 nanoseconds. Whenever I, II, and C-1, C-2, and C-3 are each of sufficient amplitude, and occur within the 200 nanosecond resolving time, a signal is sent to the scope trigger and camera advance unit. This unit triggers a Tektronix type 531 oscilloscope at the proper time to display the train of pulses from the low level mixer. This train is recorded by a 16 mm pulse camera, and the camera advance unit then advances the film one frame. If another trigger arrives before the film has advanced, it is blocked by the camera advance unit. A detailed

description of the camera and the properties of the other "blocks" in figure 9 (except the fast coincidence circuits) is given by Elliott (17).

Several scalers monitor the coincidence rates I·II and C-1·C-2·C-3; the number of oscilloscope triggers (I·II·C-1·C-2·C-3); and the number of pictures taken. The discriminator, the scalers, and the scope trigger unit are all gated off except for the short period during each machine cycle when the gamma ray beam is actually spilling out of the synchrotron.

7. Scanner. During the course of the experiment more than fifty thousand oscilloscope pictures were taken, and each picture contained between nine and fourteen pulses. In order to read, record, and process this data in a finite length of time, a Recordak Model PM-2 motor-driven microfilm reader was incorporated into a semi-automatic film scanner.

A system of mirrors is arranged inside the reader to project a bright line across a screen that also displays an image of the oscilloscope trace. One of these mirrors can be rotated through a small angle by rotating a shaft attached to a wheel on the control panel of the scanner. This shaft is also connected to a Datex shaft position encoder. By turning the wheel, the bright line may be placed anywhere across the image of the oscilloscope trace. To measure a pulse height, then, it is only necessary to turn the wheel until the line lies along the

baseline of the trace, press a button to enter the reading from the shaft position encoder on punched paper tape, then lay the line along the top of the pulse, and press the button again. For more than one pulse, it is necessary to lay the line along only the top of each pulse in turn, pressing the button each time. The paper tape may then be fed into a digital computer, which can extract the pulse heights from the encoder readings and also do any sorting or analysis necessary. This method is at least three times faster than recording pulse heights manually, but a more significant advantage gained is a great decrease in operating fatigue and concomitant reading errors.

III. EXPERIMENTAL PROCEDURE

A. General

All data for both the $\gamma + p \rightarrow K^+ + \Lambda^\circ$ and the $\gamma + p \rightarrow K^+ + \Sigma^\circ$ reactions were taken for a K^+ lab momentum of 318 mev/c. A K meson with this initial momentum was about the most energetic that the spectrometer could analyze. The number of K's reaching the rear focus of the magnet without decaying is proportional to e^{-a/p_K} where p_K is the momentum of the K meson, and already at 318 mev/c about 68% of them decay before passing all the way through the system. For this reason, it was decided to run with the highest momentum available. There were advantages to running all points at the same momentum, since then flight times, ionization losses and ranges in counters, and in general all criteria used for identifying K mesons were identical on every run. This uniformity was especially important for the points where subtractions had to be made.

As may be seen from figures 1 and 2 in Chapter I, a constant K laboratory momentum leads to an almost constant K emission angle in the center of mass system, for the region explored by the present experiment. Because of the low K counting rates the statistical accuracy of the data obtained was low enough that the small variation in C. M. angle was not objectionable.

In all, Λ° points were taken at four different photon energies, and Σ° points were taken at three different photon energies. However, the usefulness of one of the Λ° points was seriously limited because background problems made it necessary to discard most of the data at that point.

In order to avoid difficulties which might have arisen because of the rapid falling off of the bremsstrahlung spectrum near its high energy end, the peak energy of this spectrum was held at least 75 mev above the energy of those photons actually producing the K mesons being detected. Although the maximum photon energy available from the Caltech synchrotron was 1500 mev, no data were taken for which the energy of the production gamma ray itself was greater than 1400 mev.

The data accumulating process was broken up into "runs" of three different types. The first and second types, called pi_a and pi_b runs, respectively, were calibration runs using pions. In the pi_a runs, the time of flight and aperture counter delays were set in such a way that the outputs of fast coincidence circuits I and II for pions corresponded to K meson flight times. In the pi_b runs, the delays were made identical to those used when detecting K mesons so that pions registered as they would during actual K runs. For the third type of run (K run) the gains of the 522 amplifiers on C-1, C-2, and C-3 were lowered until the pulses out of these amplifiers

for K mesons passing into the telescope fell into the same range that pions occupied during the pi runs. Since all of the slow timing circuits followed these amplifiers, and since these circuits had to be timed using pion pulses, decreasing the gain to keep K pulses about the same size as the (pion) pulses used for timing avoided any pulse height effects on the timing.

For the K runs, the sum output of the time of flight chronotron was made to discriminate somewhat against pions by combining at the adder only the first two of the three undelayed diode coincidence signals from the duplexers (see figure 7d). Pion flight times were such that they favored the last two of these signals, and so some of the faster (less K like) pions were rejected. To make sure that it did not affect the fast timing calibration, no sum output coincidence from the time of flight circuit was required for the camera to trigger during the pi_a and pi_b runs.

For each run the maximum photon energy, total integrated photon flux, magnet momentum and angle, number of pictures taken, and readings of the various scalers were recorded. Calibrations of the electronics monitoring the beam energy and flux as well as checks on the spectrometer magnet settings were made periodically.

Since the discriminator biases on the slow coincidence were sitting on the steep upper slope of the pion distribution during the

K runs, and since most of the I·II·C-1·C-2·C-3 coincidences were pions, even in the K runs, any change in the pion pulse spectrum from a given counter, as seen at the discriminator, would show up in the slow coincidence rate. Consequently, the coincidence rate for K runs was fairly sensitive to changes in the counter telescope electronics. As most of the K runs contained about 200 I·II·C-1·C-2·C-3 events, the statistical standard deviation of the coincidence rate was about the same for each run. It was possible, therefore, to estimate this standard deviation from the first few runs at a given K point and require that all the subsequent rates at that point fall within three standard deviations of the average rate observed on the first few runs. This is the usual "quality control" criterion. By interspersing the first runs at a new point with runs at an old point, it was possible to make sure that no shifts in the pion spectra occurred between the runs at different points. The statistical technique proved useful on occasions when the target or the beam monitoring system were disturbed by other personnel during the course of a run. In each case where the coincidence rate was more than three standard deviations from its average value, some such disturbance was found.

As another check on the gains associated with each counter, the counter spectra for pions as seen by the discriminators on the slow coincidence chassis, and also the discriminator biases, were measured occasionally with a twenty channel pulse height analyzer.

These checks on the counter pulse heights at the slow coincidence made it possible to determine that the slow coincidence circuit was triggering the camera on each suitable event.

After each several runs, the film from the oscilloscope camera was developed and labelled. Later this film was scanned and its pulse height information transferred to punched paper tape.

B. Calibrations

For the K meson runs, it was necessary to know the ratio of the energy loss in each counter of the counter telescope to the corresponding pulse height from that counter. It was also necessary to have an accurate determination of the flight time of the K mesons through the system. These quantities were determined by measuring the response of the apparatus to a particle (the pion) with known energy losses and a known time of flight and then estimating the response to K mesons, using the theoretical relationship between the energy loss of a particle and its total energy, and also using the (experimentally verified) linearity of the time of flight parameter T with flight time. It is necessary to correct for a small non-linearity in the relationship between energy loss and scintillator light output for particles near the end of their range (18).

Using pions, the counter high voltages and amplifier gains were adjusted until the heights of the pulses at the input to the discriminators were in the right range to trigger them properly. The phototube high voltages were set only high enough that the anode pulse

from each phototube could operate its fast coincidence circuit reliably (see below). This was done to prevent saturation of the phototube output pulses on large signals. In every case it was possible to run the high voltage several hundred volts higher before saturation occurred on pion pulses. Since the phototube output pulse height approximately doubles for each hundred volt increase in the high voltage, it was certain that the phototube was linear over the range of pion and K meson pulse heights used. Even in C-3, the stopping counter, the K pulses were only about four times as high as the pion pulses. As an added precaution against saturation, the signals used for pulse height analysis were taken out four dynodes before the anode in C-1, C-2, and C-4, and two dynodes before the anode in C-3. As the light output from C-3 was quite large, it was possible to operate its phototube in such a way as to optimize its linearity, with some loss of gain, by using a so called "high current" voltage divider to supply the dynode voltage to the phototube (19).

In F-1, F-2, V-1, and V-2, the high voltages were also kept low in order to cut down on accidental coincidences from small random pulses.

Checking high voltages was done by connecting one of the fast coincidence circuits in such a way that pions passing through two counters to be checked would produce a spectrum of pulses from its sum output. This spectrum would be displayed on a pulse height

analyzer and then the high voltage to one of the input counters would be reduced until this spectrum started to deteriorate. The voltage would then be increased again by about 100 volts. The same procedure would then be followed for the other counter. It was, of course, important to run a delay curve at each voltage tried, since the time measurement changed about 2 nanoseconds with each 100 volt change in the high voltage, and this would also cause the sum output spectrum to deteriorate.

Typical pion spectra for C-1, C-2, and C-3 are shown in figures 10 and 11. (The spectrum for C-4 is not shown, since because its calibration was not critical, the pulse height in C-4 was not read from the film. Runs using the pulse height analyzer show that its spectrum is slightly narrower than that of C-2). Notice that pulses more than three times the height of the pion peak are present. In the spectrum for C-3, there is a saturation bump for very high pulses. By changing the attenuation at the input to the pulse amplifier and noticing that this bump remains stationary while the pion peak does not, it is easy to show that the saturation occurs in the amplifier and not before it. Since during K runs the pulses are attenuated to approximately the same height as pi run pion pulses before entering the amplifier this saturation does not affect K spectra any more than it does those of pions. The pulse amplitude at

FIGURE 10

TYPICAL PION PULSE HEIGHT SPECTRA FROM C-1 AND C-2

Data taken from a set of pi_a and pi_b calibration runs. Spectra shown include any spread introduced by scanning or drift. Units of pulse height are arbitrary.

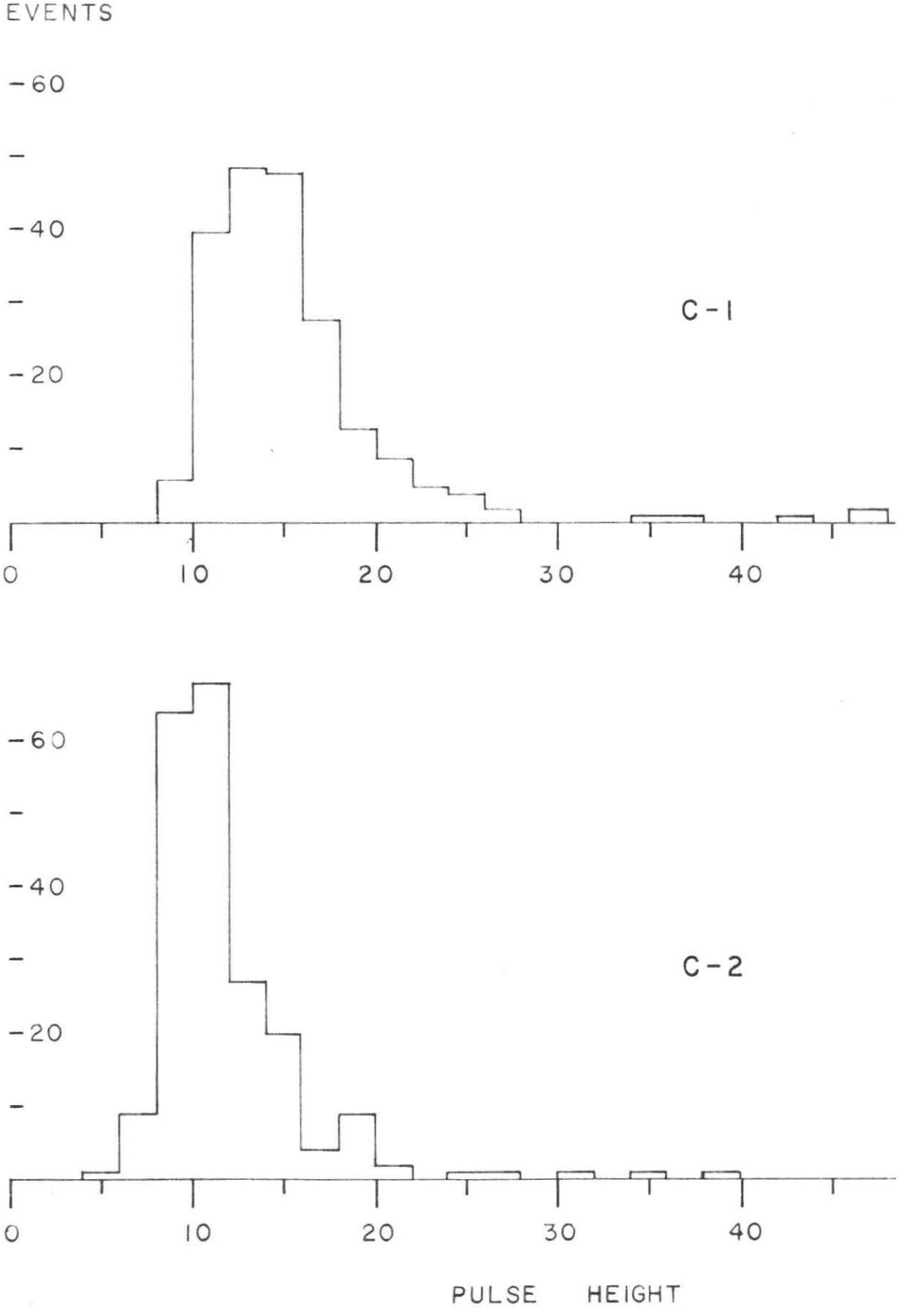
EVENTS
60
40
20
0
10
20
30
40
C-1
60
40
20
0
10
20
30
40
C-2
PULSE HEIGHT

FIGURE 11

TYPICAL PION PULSE HEIGHT SPECTRUM FROM C-3

Data taken from a set of pi_a and pi_b calibration runs. Spectrum shown includes any spread introduced by scanning or drift. Units of pulse height are arbitrary.

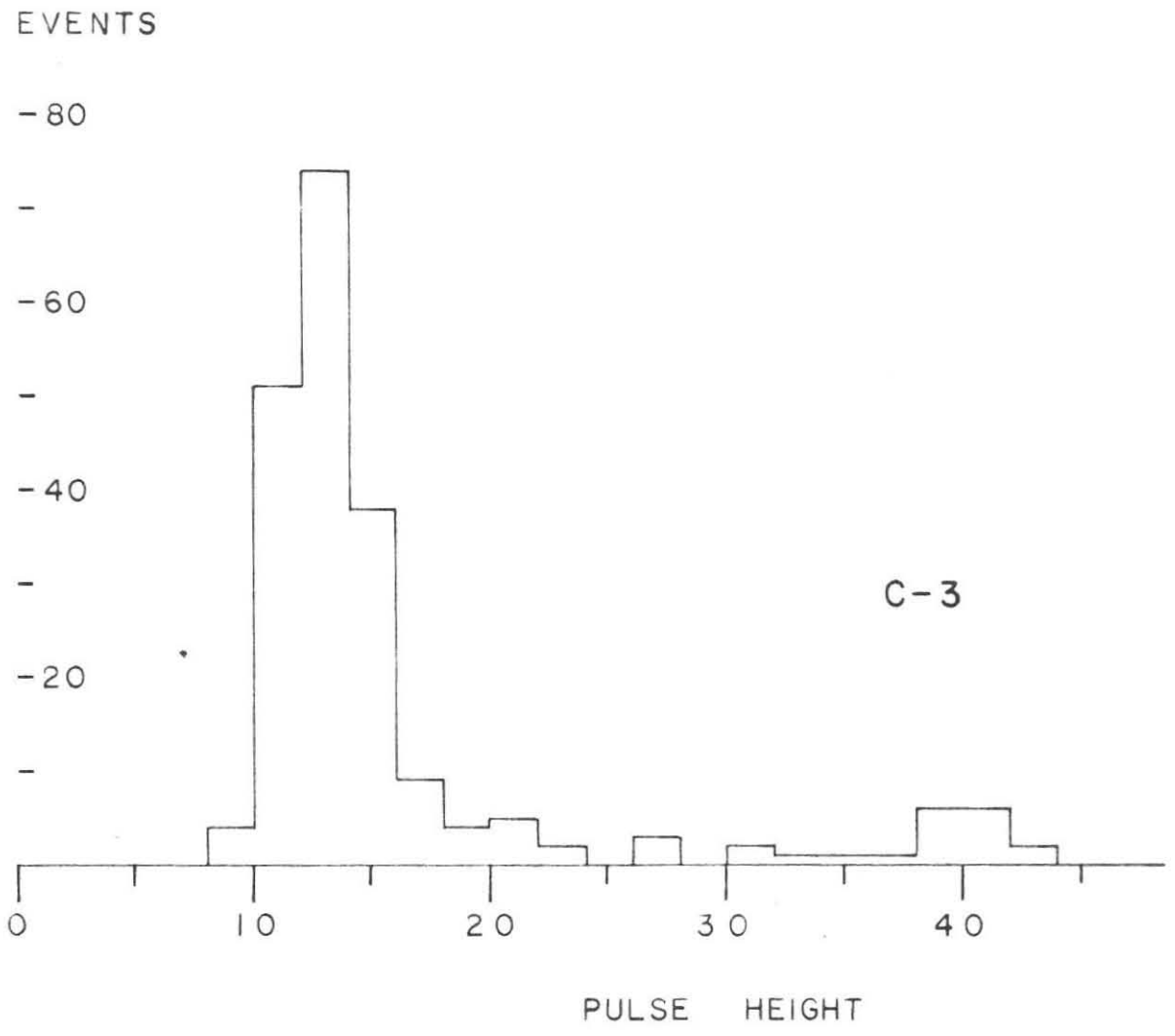
EVENTS
80
60
40
20
C-3
0
10
20
30
40
PULSE HEIGHT

which this bump appears agrees with what one would expect from the characteristics of the amplifier, and can also be seen using a pulse generator.

The average value of the pion spectra from the pi_a and pi_b runs remained constant within statistics for each continuous set of runs. There were about fifty events in each determination of a spectrum. Statistical tests for unilateral drift in this average value gave negative results (20).

As experience was gained with the scanning, various changes were made in the magnification and scaling factors between the actual pulse height on film and the number recorded on paper tape. Also, changes were made from time to time in the actual pulse heights recorded on the film. These changes always, of course, defined a new set of runs. There were in all six sets of runs. Since information used to identify K mesons was always obtained by comparing it with the relevant pion calibration runs, the existence of these different sets was only annoying. None of these changes affected the slow coincidence rates, of course, as they were made beyond the slow coincidence circuitry. Since the fast timing depended only on ratios of pulse heights, it also was not affected.

The efficiencies of C-1, C-2, C-3, and C-4 for pions were checked by displaying the spectra of the individual counters on a pulse height analyzer with the bias for that counter set much

lower than normal for pions. So few pulses occurred below the normal biases that an efficiency of 100% could be assigned to each counter.

The fast timing on the time of flight and aperture counters was set up by using the sum outputs of chronotrons I and II as 12 nanosecond resolution coincidences and running delay curves for pions. The complete spectrum of the sum output was recorded at each delay setting and used to help determine the exact center of the delay curve. This could be done to within a nanosecond. These spectra also showed where to set the bias on the sum output signal in order not to miss any events with the proper time of flight. At the bias settings used, a sum output signal was present for more than 99% of the pions traversing the system. The other fraction of a percent could be accounted for by contamination of the beam, or by counter dead time, so an efficiency of 100% was assigned to the sum outputs of the chronotrons.

Final fast timing was done from the pi_a, pi_b, and K runs themselves. The triplet output of each of the chronotrons was reduced to a value of the time parameter T discussed earlier. The distribution of this parameter for a typical set of pi_a and pi_b runs is shown in figure 12 for T_I and in figure 13 for T_{II}. By taking these runs for two different delays, i.e., the pi_a and pi_b case, it was possible to monitor for changes in the slope of the linear T

FIGURE 12

TYPICAL SPECTRA OF PION TIME OF FLIGHT PARAMETER, T_I

The pi_a run delay setting differs by 7 nanoseconds from the setting for the pi_b runs.

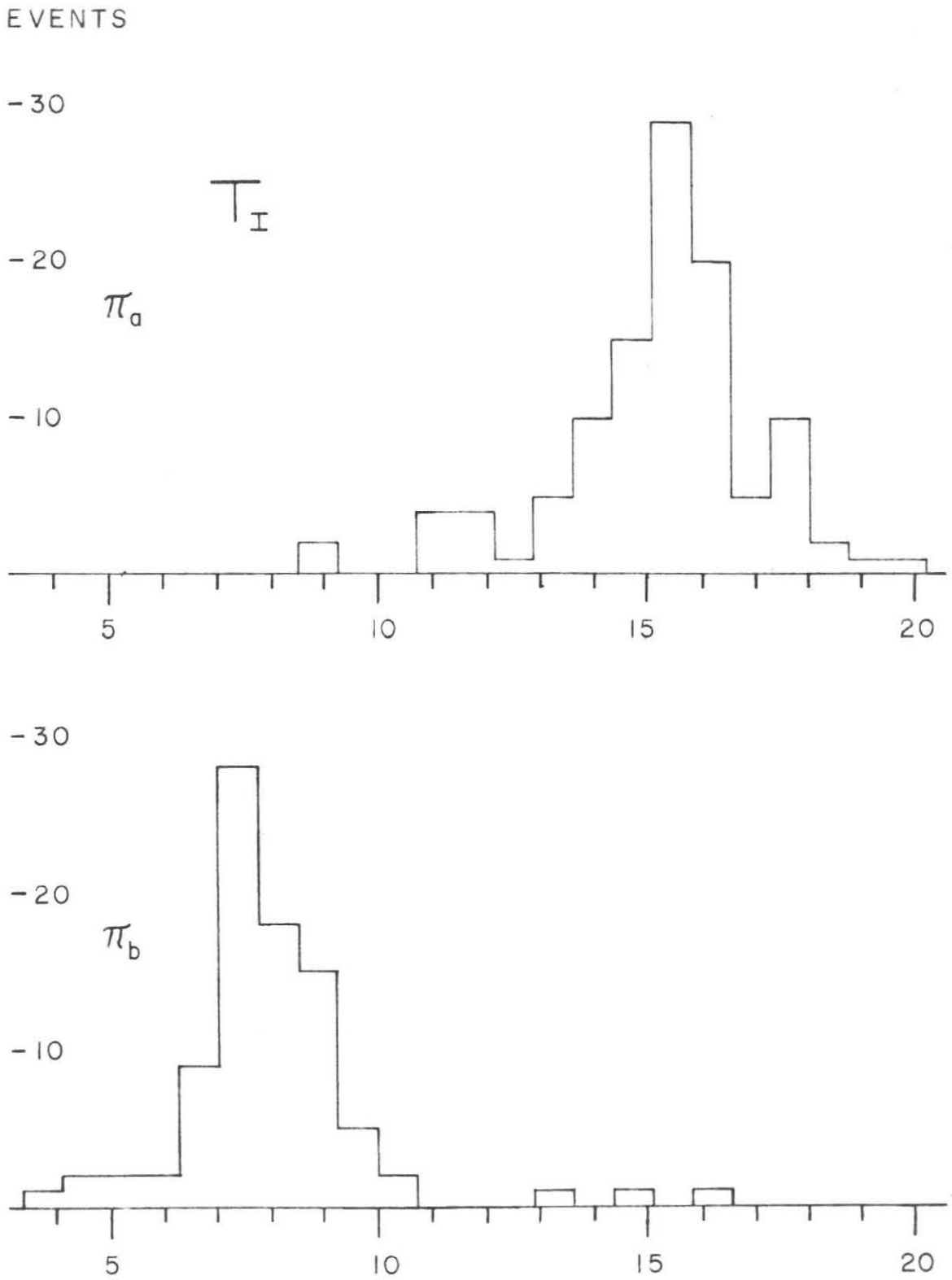
EVENTS
-30
-20
-10
T_I
π_a
5
10
15
20
-30
-20
-10
π_b
5
10
15
20
TIME OF FLIGHT (nanoseconds)

FIGURE 13

TYPICAL SPECTRA OF PION TIME OF FLIGHT PARAMETER, T_{II}

The pi_a run delay setting differs by 5 nanoseconds from the setting for the pi_b runs. Scale shown only for the range of T_{II} in which it is approximately linear with time.

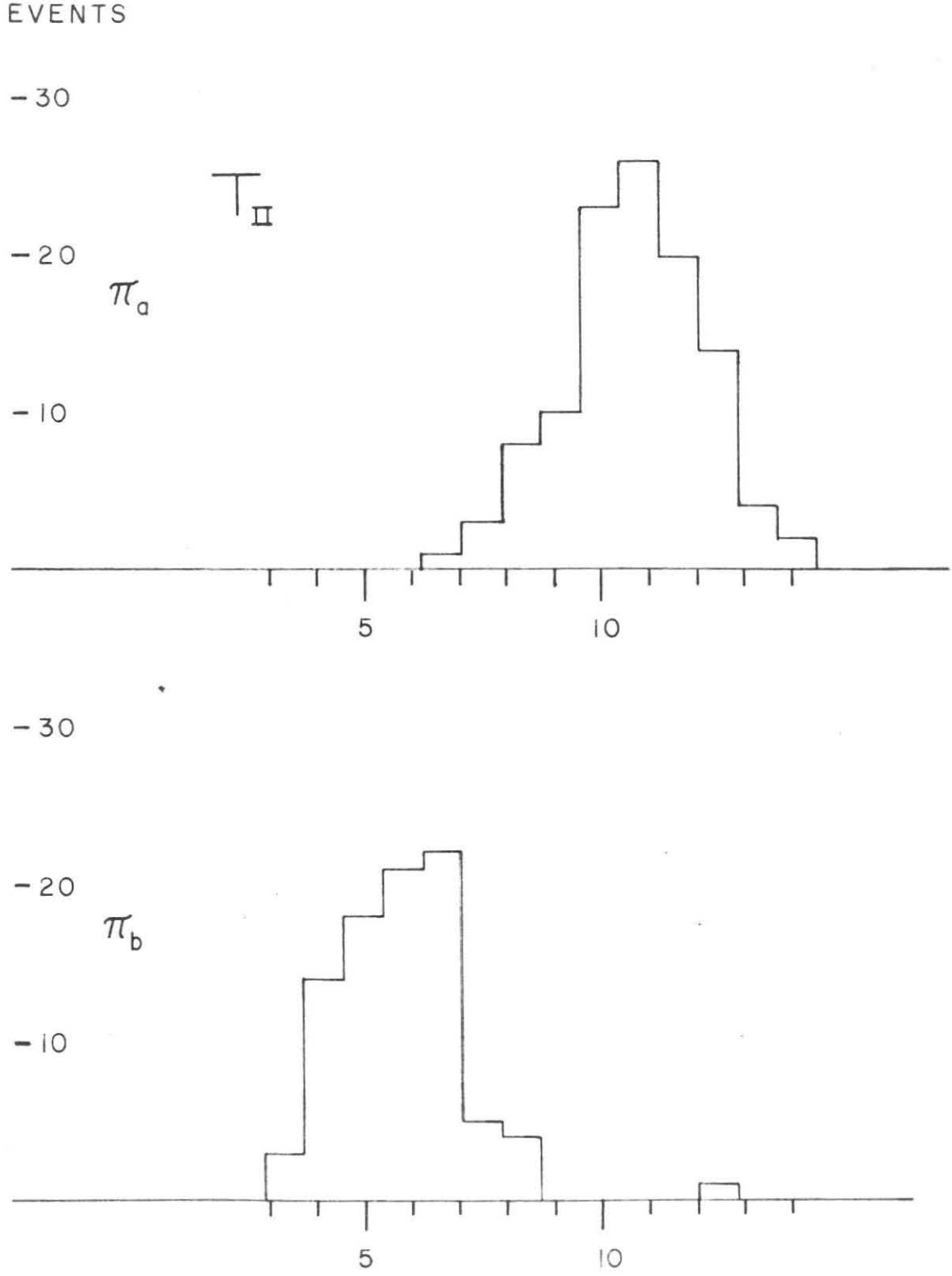
EVENTS
-30
-20
-10
π_a
5
10
-30
-20
-10
π_b
5
10
TIME OF FLIGHT (nanoseconds)

versus time relation, as well as for simple displacements of T with respect to time. As mentioned earlier, the chronotrons proved so stable that no statistically significant change in the average values of either T_I or T_{II} for the pi_a or pi_b runs was ever found.

Pions were used to check the performance of the fan vetos, V-1 and V-2, and to set up their timing and high voltage. The fraction of pions showing a veto pulse on the pi_a and pi_b runs remained constant at 16 % throughout the experiment. During the calibration runs, the effectiveness of each element of the apparatus in eliminating pions when running under K conditions was measured. It was found that C-1 or C-2 by themselves would eliminate about 80 % of the pions, while C-3 would eliminate 90 % of them. The rear counter, C-4, also eliminated about 90% by itself. If C-1, C-2, and C-3 were statistically independent, C-1·C-2·C-3 should should eliminate 1 - .20 x .20 x .10 or 99.6 % of the pions. Actually, the number is closer to 97 % . Only about half of this three percent remaining pass out through C-4 and are vetoed. So about ten or fifteen pions per K meson are left to be eliminated by the fast timing. A quarter of these are thrown out by the sum outputs of the chronotrons, and it is necessary to resort to analysis of the oscilloscope pictures, and in particular, the time of flight triplet, to complete the separation of K's from pi's. The residual background rate is about 15 % of the K meson counting rates.

One other necessary calibration was that of the solid angle subtended by the magnet-counter system at the hydrogen target. The anti-scattering counters V-1 and V-2 used in place of the lead strips which originally defined the horizontal solid angle were designed to allow use of a somewhat larger solid angle than the nominal solid angle of the magnet. This new solid angle could be calculated using the known changes in geometry, along with data available from previous measurements on the magnet (15). It was felt advisable to check the new solid angle using the known cross section for positive pions. This calibration is discussed in Appendix I.

C. Scanning

Immediately after development, each film from the oscilloscope camera was examined for photographic or electronic mishaps. Each run on the film was classified as either a pi_a run, a pi_b run, or a K run. On the pi runs the scanner was instructed to read each trace. On the K runs, only those traces having T_I greater than minus one and no pulses from either C-4 or the coincidence circuit on the antiscattering counters were read. The traces that were not read on these K runs were identified on the paper tape as either vetoed events (C-4 and/or an antiscattering pulse present) or as events with pi-like values of T_I. In this way, a tally of the total number of traces read in each run could be made later by the computer program. This tally could then be checked against the

FIGURE 14

SAMPLE OSCILLOSCOPE PATTERNS

a) Pion from a pi_b run (K run timing and pi run gains).

b) K meson from a K run.

c) Pion from pi_b run with pulse from "fan counter" coincidence circuit.

d) K meson from a K run with pulse from "fan counter" coincidence circuit.

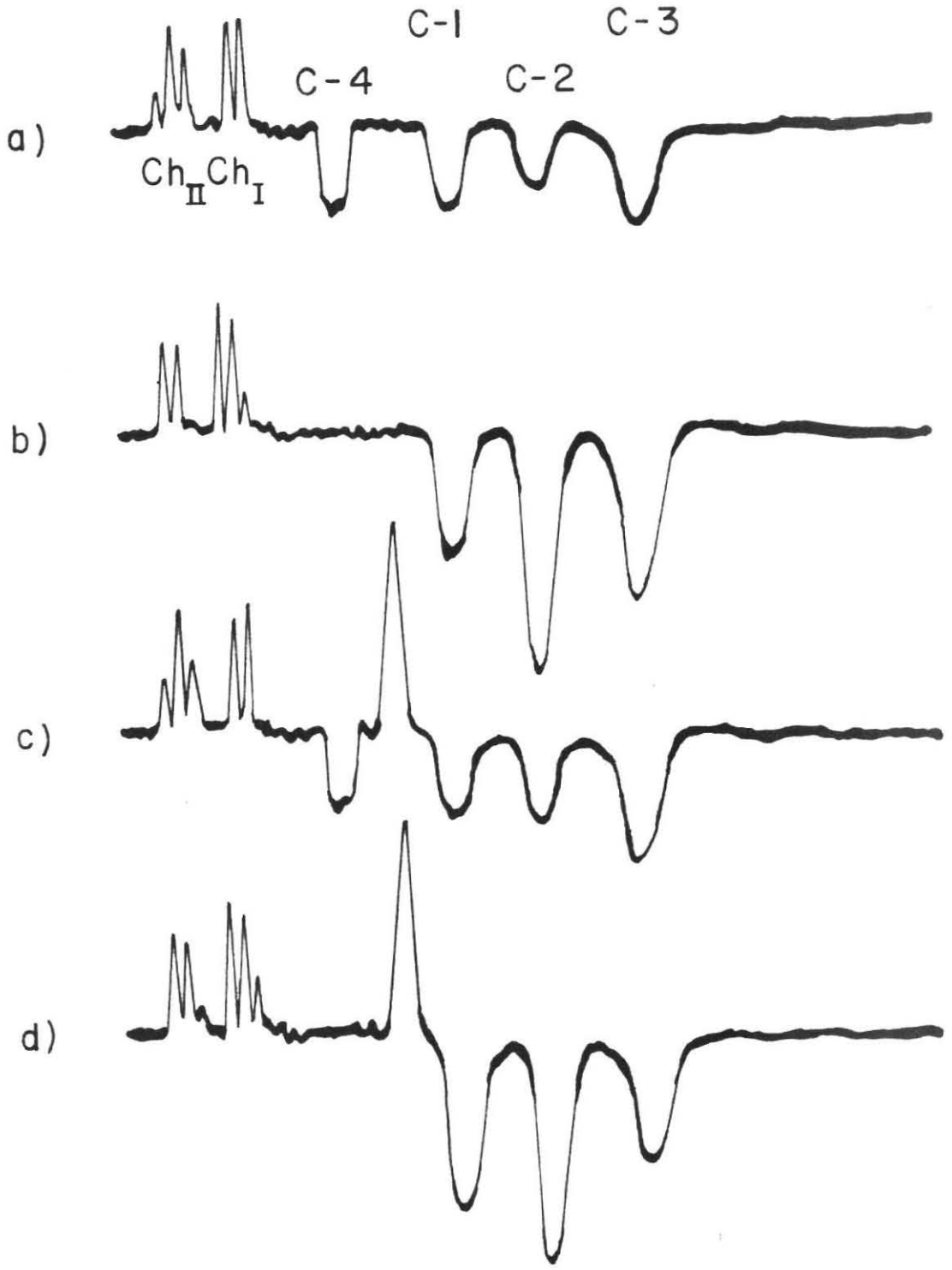
C-1
C-3
C-4
C-2
a)
Ch_{II} Ch_{I}
b)
c)
d)

number of pictures actually taken, as recorded by the register on the camera advance unit. Since only one trace could be recorded in each picture because of the oscilloscope trigger lockout in the camera advance unit, the trace tally from the computer should agree with the picture tally. If it didn't, it was necessary either to re-read the film or to find the scanner's error by looking at the tabulation of pulse heights printed out by the computer program. Provision was available in the scanning format for the scanner to record the fact that a particular trace was not readable for some reason, or that a trace had not registered in a particular frame of the film. This information was needed in the tally mentioned above.

Three types of scanning errors occurred: omission of a trace, recording the same trace twice, and inaccurate reading of a pulse height. Two types of checks were made on these sources of error, the first being the tallies mentioned above, and the second being the comparison of the results from sets of runs that were scanned two different times. Both checks showed omissions to be completely negligible. Duplication of the same trace occurred on about 5 % of all the runs. This meant that there was about a 2 % chance that a trace from a K meson would be duplicated. Most of these, however, were easily caught and eliminated by the tally check. If the tally of a given run wasn't correct, the computer tabulation of the information from that run was examined, and it was

quite easy to find duplicate, adjacent entries, and eliminate them before the data was analyzed further. Reproducibility of the pulse height readings was within the width of the base line of the oscilloscope trace, or about 5 percent.

A check on the spread introduced in the pulse height spectra by the combination of scanning errors and gain drifts can be obtained by comparing pion pulse spectra obtained by combining information scanned from the films of several days of running with pion spectra obtained in a few minutes using a pulse height analyzer. These comparisons show no noticeable difference between the widths of the two spectra. (Counter C-3 had the best resolution for pions, and the standard deviation of its pion spectrum was typically 12 to 15 percent.) It is possible to say from these comparisons that pulse height error introduced by the scanning and drift combined is between zero and 7 or 8 percent.

D. Identification of K Mesons

All K run events that were sufficiently K-like in their properties to satisfy the electronic biases and scanning criteria were fed into the Caltech Datatron 220 digital computer to be analyzed further. The computer was programmed to calculate T_I and T_{II}, the time parameters, to make histograms of any of the pulse heights of interest, as well as of T_I and T_{II}, and to make two dimensional histograms ("dot plots") of any pair of the above

quantities. In addition, it was possible to set upper and lower biases on any or all of the set of quantities associated with each event, and to make either a histogram or "dot plot" from only that subset of events satisfying these biases. For example, it was possible to make a "dot plot" of, say, C-2 versus T_I for all events with T_{II} greater than zero, and C-1 and C-2 greater than some $C\text{-}1_{min}$ and $C\text{-}2_{min}$, respectively. The average value and the variance were automatically calculated for each histogram. Upper and lower limits as well as the channel widths could be selected for each histogram.

Using the pion calibrations, the properties of the scintillation counters, the theory of ionization losses, and the measured properties of the attenuator in the input to each pulse amplifier, it was possible to calculate the expected pulse height distribution for K mesons from each counter. These calculations were used to set the electronic biases that determined which events were photographed, and also to help determine which events recorded on film were actually K mesons. In C-1, the K peak was predicted to occur at 2.70 times the pi peak, and in C-2 the K peak should occur at 3.00 times the pi peak. A clear K peak was not expected in C-3, since the K's stopped in this counter and decayed into various fast and slow light particles. The average K pulse height expected in C-3 was about 4.4 times the pion peak in this counter.

Light decay products from the stopping K's tend to increase this average by about 20% . The minimum acceptable K pulse height in C-3 was chosen to be 4.4 times the minimum acceptable pion pulse height.

In figure 15 are shown typical spectra in the three counters for events whose fast timing characteristics would identify them as K mesons. The lower end of the spectrum in C-3 is close enough to the value of the electronic bias used that there is some question as the whether or not some of the K mesons may have been biased out electronically. Because of its smeared out nature, it was never possible to establish the lower limit of the K spectrum in C-3 from the K data. Since most pions that were photographed were those which penetrated as far as C-3 and then were absorbed, producing a whole continuum of pulse heights, the pion background in C-3 also interfered seriously with attempts to establish this lower limit. As a result, it was necessary to rely on calculations using the pion data to establish this limit and to find the efficiency of C-3 for K mesons. To check on the bias problem, a set of K runs was made with reduced electronic biases. The results of these runs indicate that there may have been an over-all loss of efficiency in the original runs because of electronic biases of from zero to as much fifteen percent. The uncertainty in this loss of efficiency contributes to the error in the absolute value of the cross sections measured in

FIGURE 15

COUNTER SPECTRA FROM K MESONS

Pulse heights are expressed in terms of the same arbitrary units used in figures 10 and 11 for the pion pulse spectra. These units are a measure of the relative heights of the various pulses before amplification. The distance from the origin along the abcissa in each of the plots of figure 15, and also in figures 10 and 11, is proportional to the pulse height after amplification. The spectra after amplification are seen to be approximately the same for the kaon and the pion pulses.

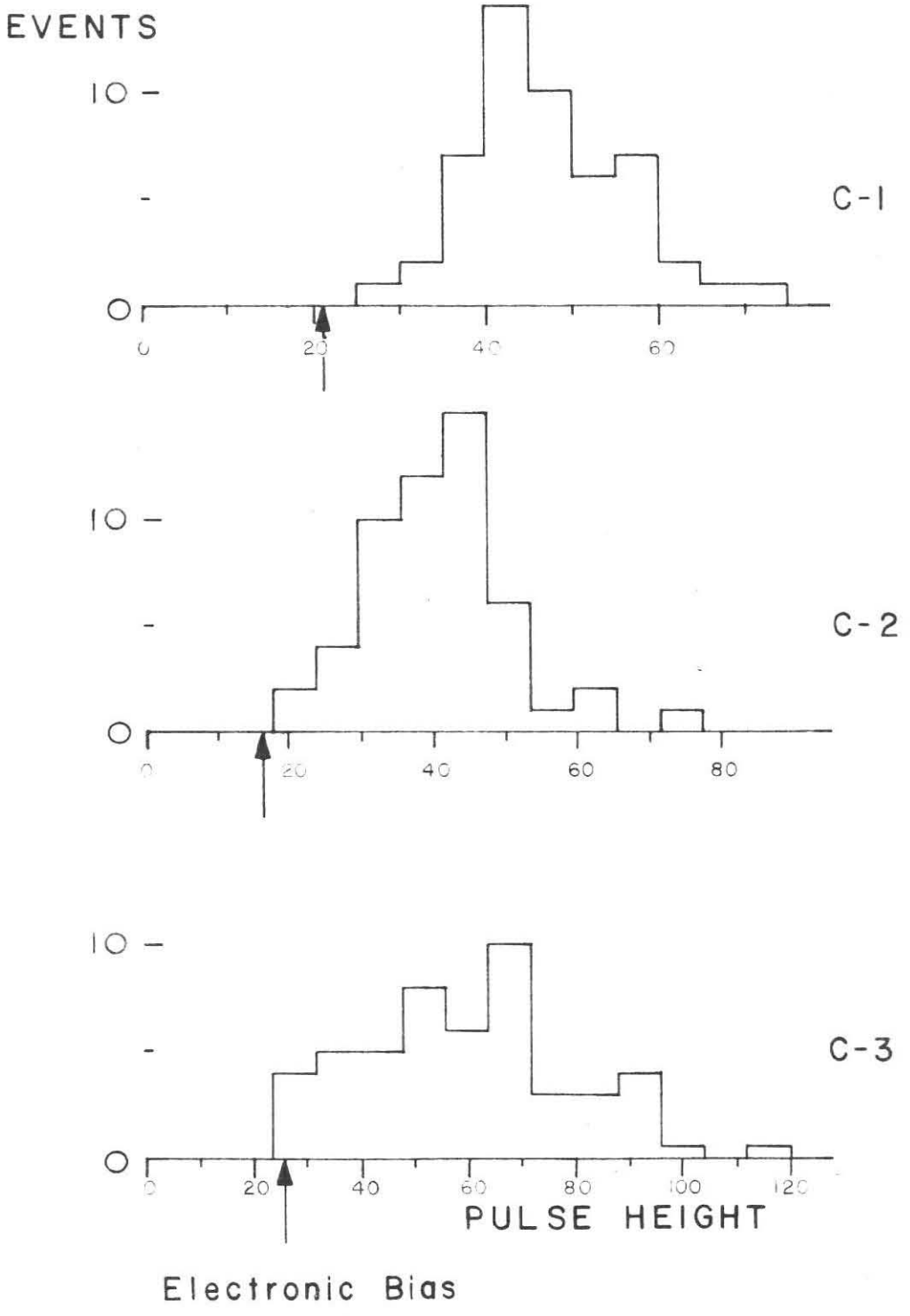
EVENTS
10
0
C-1
0
20
40
60
10
0
C-2
0
20
40
60
80
10
0
C-3
0
20
40
60
80
100
120
PULSE HEIGHT
Electronic Bias

this experiment, but has a negligible effect on relative cross sections, as the biases, relative to pion pulse heights, were the same throughout the experiment.

Final values of the cross sections stated may be as much as 15 percent too low because of the above mentioned loss of efficiency. Unit efficiency was assumed in reducing the data.

The position and shape of the time of flight spectrum predicted for kaons is shown in figure 16. The position of the curve shown was calculated using the known position of the pion time of flight peak and the T versus time curve of figure 9. Allowance has also been made for the fact that the time of flight measurement is somewhat pulse height sensitive. A rough measurement may be made of this sensitivity by increasing the height of the pulse feeding the time of flight by a known amount using the high voltage on the photomultiplier tube producing the pulse. This gives a shift in the value of the time of flight measurement, but only part of this shift is due to the change in pulse height, the rest arising from the fact that the transit time of the signal through the photomultiplier itself is decreased by increasing the high voltage. The second effect can be estimated fairly well, and allowed for (19). In the present case, the total time shift between normal pion flight times and "K" flight times simulated using the above method was 2.0 ± 0.3 nanoseconds, and the

contribution of the transit time through the tube to this value was estimated to be 0.9 nanoseconds, leaving a net shift of 1.1 nanoseconds.

The shape of the curve shown in figure 16 includes contributions from three effects: the different path lengths available to the K mesons through the magnet, the finite momentum acceptance of the magnet, and the finite resolution of the time of flight circuit, as determined using pions.

No difficulties arose with the electronic or scanning biases used on the timing measurements. The experimental results exhibited in figure 16 for T_I are all derived from information which passed both biases and was presented to the computer. The bias used in reducing the data is indicated in the drawing, and is seen to be well within the electronic and scanning biases, whose effect is beginning to become apparent only at the extreme left hand edge of the plot.

Similar results were obtained for the timing of the aperture counter, although of course the separation between pions and K's is not as great. Using the predicted resolution curves to calculate the efficiency of T_I and T_{II} combined gives a value of 0.93, and this value was used to reduce the data.

As was mentioned earlier, the time of flight measurements were extremely stable during the entire course of the

FIGURE 16

TYPICAL K MESON TIME OF FLIGHT SPECTRUM

Shown are the predicted and the measured spectra of the quantity T_I, reduced to nanoseconds. The data shown satisfy the condition that they are K-like in C-1, C-2, and C-3. The experimentally determined position of the pion peak is shown, as well as the value of the bias used for T_I in reducing the data. The dotted histogram represents the T_I spectrum from a below threshold run, normalized to allow for the effect of the different bremsstrahlung end point energy used for the below threshold measurements.

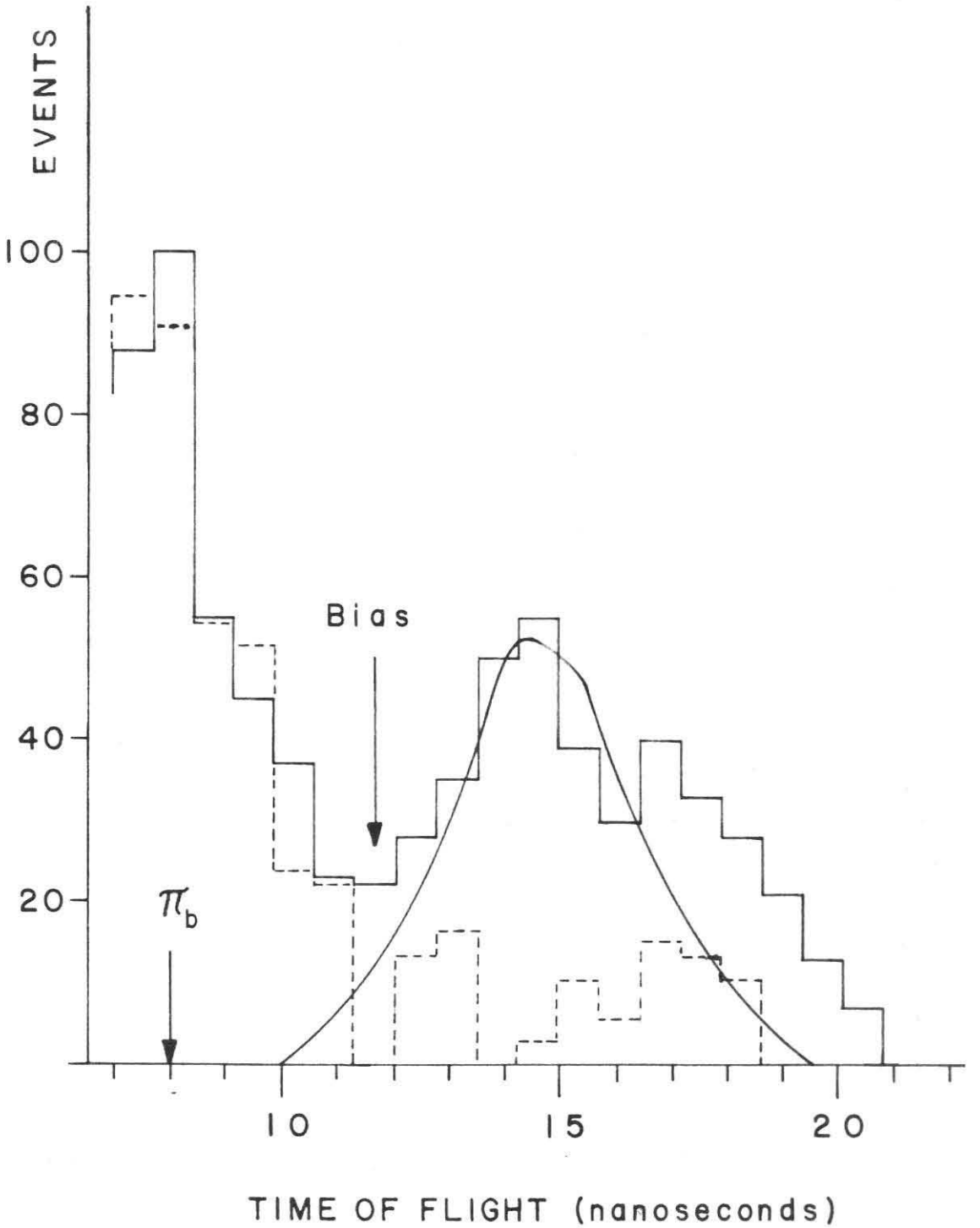
EVENTS
100
80
60
40
20
Bias
π_b
10
15
20
TIME OF FLIGHT (nanoseconds)

experiment, and were a very necessary part of the identification of the particles detected as K mesons.

E. Backgrounds

To determine the true K-counting rates from hydrogen, the counting rates from "K runs" below the thresholds for the production of K mesons in hydrogen were subtracted from the observed K rates above threshold. The geometry of the experiment was such that only a small number of the events detected originated outside the hydrogen of the target. This was confirmed by taking K runs with the target empty. The counting rate for these runs was much less than the rate on the below threshold runs so that it was appropriate to use below threshold runs for "background" rates. The K-like events appearing in the below threshold runs come from two sources: First, pions produce proton stars in C-1 and the protons from many of these stars have the proper range to penetrate C-2 and stop in C-3, simulating kaons; and second, some fast protons may still have passed through the magnet with the wrong momentum by scattering from the pole tips. Calculations show that a significant contribution to the below threshold rates is possible even allowing for the inefficiency of the time of flight circuit for pi mesons on the K runs. Some evidence for the second process appears in figure 16 in the form of the apparent excess of events with times of flight around

18 nanoseconds. This is also the time of flight range of the protons which will best simulate K mesons in the counter telescope. A few of the below threshold runs showed small time of flight peaks in this region.

Below threshold counting rates are given in Chapter IV.

IV. CROSS SECTION CALCULATION

A. General

The basic equation for calculating a cross section from the measured counting rates, the various properties of the instrumentation, and the kinematics of the reaction involved is:

$$\sigma(k,\theta') = C \left[R\, d\, n(k)\, \Delta k\, \frac{\partial \Omega'}{\partial \Omega}\, \Delta \Omega \right]^{-1}$$

where

$\sigma(k, \theta')$ is the center of momentum differential cross section,

C is the net K counting rate (per kilobip),

R is a factor to include corrections for decay, absorption, detection inefficiency, etc.,

d is the average number of protons in the beam, per cm^2,

$n(k)\, \Delta k$ is the number of photons with energy in Δk, at k, per kilobip,

Δk is the range of energies of the photons producing the K mesons entering the detector,

$\frac{\partial \Omega' \Delta \Omega}{\partial \Omega}$ is the solid angle acceptance of the detector in the center of momentum system.

The net counting rate C is the difference between the counting rates for full target runs above and below threshold, with allowance made for the fact that the "bip" and the bremsstrahlung spectrum depend on the peak synchrotron energy E_o.

The quantity R is discussed in section C of this chapter.

Using a density of 0.0707 gm/cm^2 for liquid hydrogen and an effective thickness of 7.18 cm for the hydrogen volume in the photon beam, d is found to be 3.034 x 10^{23}/cm^2.

As mentioned in Chapter II, $n(k)\,\Delta k$ is usually presented in the form:

$$n(k)\,\Delta k = \frac{W}{E_o}\, B(E_o, k/E_o)\,\frac{\Delta k}{k},$$

and we note that W depends somewhat on E_o. Since it is the momentum acceptance of the spectrometer system Δp, rather than Δk that is actually held fixed in the experiment, it is convenient to write:

$$\Delta k \simeq \frac{\partial k}{\partial p}\,\Delta p\ .$$

To express Δp in terms of the central momentum at the magnet, p_o, we may write:

$$\Delta p = \frac{dp}{dp_o}\,\frac{\Delta p_o}{p_o}\,p_o$$

where dp/dp_o can be calculated from the ionization losses between the target and the center of the magnet, and is equal to 0.714 (p_o was held fixed at 273.0 mev/c).

It is useful to define a function $G(p,k)$ such that:

$$\beta^2 G(p,k) = \frac{\partial k}{\partial p} \frac{\partial \Omega'}{\partial \Omega}$$

(β is the K meson velocity corresponding to p, and β^2 equals 0.293). This function varies quite slowly with p and k, which $\frac{\partial k}{\partial p}$ and $\frac{\partial \Omega'}{\partial \Omega}$ do not.

We can now rewrite our basic equation as:

$$(k,\theta') = C\left\{\left[\frac{W\, B(E_o, k/E_o)}{kE_o}\ G(p,k)\right]\ \left[R\, d\beta^2 \frac{dp}{dp_o} p_o \frac{\Delta p_o}{p_o}\ \Delta\Omega\right]\right\}^{-1}$$

From appendix I, $(\frac{\Delta p_o}{p_o} \Delta\Omega)$ is 0.00163 steradians.

Notice that in this last equation the first term enclosed in brackets inside the braces is the only one that differs from data point to data point, aside from the counting rate, C. This is a result of having taken all data at the same laboratory momentum, p. The other bracketed term inside the braces was then an "instrumental constant" that remained fixed throughout the experiment.

B. Background Rate Normalization

To determine the final values of the cross sections, it is necessary to subtract the contribution of the below threshold runs

from the total counting rates. Care must be taken to allow for the fact that the counting rates for the processes occurring below threshold depend on the peak synchrotron energy E_o through $n(k)\,\Delta k = \frac{W(E_o)}{E_o} B(E_o, k\ E_o)\Delta k$. Thus if the cross section for the below threshold process is σ'_b, and the counting rate at peak energy E_o^* (below threshold) is $C_b(E_o^*)$, we have:

$$C_b(E_o^*) = \sigma'_b \left(R\, d \frac{d\Omega'}{d\Omega}\ \Delta\Omega \frac{\Delta k}{k}\right) \frac{W(E_o^*)}{E_o^*} B(E_o^*,\ k/E_o^*) .$$

At some higher peak synchrotron energy, E_o, the contribution of the below threshold process to the total counting rate will be $C_b(E_o)$ or:

$$C_b(E_o) = \sigma'_b \left(R\, d \frac{d\Omega'}{d\Omega}\ \Delta\Omega\ \frac{\Delta k}{k}\ \frac{W(E_o)}{E_o}\right)\ B(E_o,\ k/E_o)$$

so

$$C_b(E_o) = C_b(E_o^*)\ \frac{W(E_o)}{W(E_o^*)}\ \frac{E_o^*}{E_o}\ \frac{B(E_o,\ k/E_o)}{B(E_o^*,\ k/E_o^*)} .$$

Most of the below threshold counting rate for the Σ° runs arose from actual K mesons produced in the $\gamma + p \rightarrow K^+ + \Lambda^\circ$ reaction, so that the photon energy, k, in the above equation could be determined from the kinematics of the Λ° process. The below threshold counts for the

Λ° runs were assumed to come primarily from pions produced in the process $\gamma + p \rightarrow \pi^+ + n$ and the value of k determined from the kinematics of this reaction was used in reducing the data. This procedure for the Λ° runs is justified by the fact that more than two-thirds of the positive pions entering the magnet aperture were produced in the above reaction, and also by the fact that $B(E_o, k/E_o)$ is a slowly varying function of k in the range of k interest.

C. Corrections

The quantity R mentioned in section A contains decay and absorption corrections to the counting rate and does not depend on k or θ.

Correction for K mesons which decay while passing through the magnet-counter system accounts for the largest part of R. Three types of events must be considered in calculating decay corrections: K mesons that decay on their way through the magnet to the detecting counters and, because of their decay, are lost; K mesons that decay on their way through the magnet to the detecting counters whose decay products pass through these counters in such a way that the event can not be distinguished from an ordinary K event, and are thus counted as K's; and K mesons that pass through the magnet which would ordinarily miss the counter telescope at the rear

focus of the magnet by a small amount, but whose decay products pass through the detecting system in such a way that the event is not distinguishable from an ordinary K event. The latter two classes of event can occur because the counter telescope, by itself, can not always distinguish a K meson from one of its decay products. Thus, if an incoming K travels far enough through the magnet before decaying that its flight time is K-like, it may be counted as if it were an ordinary K event.

Correction for K mesons that decay before stopping in the counter telescope is quite straightforward, since the lifetime of the K mesons, as well as their velocity and path length is well known. The fraction, f, of particles of lifetime τ that remain after time t is $e^{\frac{-t}{\gamma\tau}}$ or if the particles traverse a distance L with momentum p,

$$f = e^{-\frac{mL}{p\tau}}$$

where m is the mass of the particle at rest. If, then, the particle travels distance L_1 with momentum p_1, L_2 with momentum p_2, etc., we should write

$$f = \exp\left\{-\frac{m}{\tau}\left[\sum_i \frac{L_i}{p_i}\right]\right\}$$

If the probability density for a given total path L ($=\sum_i L_i$) is $P(L)$, we then have

$$R_d = \int P(L) \exp\left\{ - \frac{m}{\tau} \sum_i^n \frac{L_i}{p_i} \right\} d^n L_i$$

where R_d is the fraction of the incident particles that reach the detector before decaying. The above form of R_d is useful since in the present case, the velocity decreases as the K meson passes through F-1, and again as it passes through F-2. Also, the lengths of the various flight paths available to the mesons passing through the system are not the same. The above integral may be evaluated by finding $P(L)$ from the properties of the magnet, and using Simpson's rule.

Because the counter telescope measured range as well as dE/dx, and because the decaying K mesons were going fairly slowly ($\beta = 0.49$) and decayed mostly into two fast (β greater than 0.9) particles, only one of which was charged, the contribution of the second and third processes mentioned above to the decay correction is quite small. The significant decay modes of the K^+ meson along with their branching ratios are:

1.	$\mu^+ + \nu$	58 percent
2.	$\pi^+ + \pi^\circ$	25 percent
3.	$\pi^+ + \pi^- + \pi^+$	6.2 percent

4.	$e^+ + \nu + \pi^\circ$	5.1 percent
5.	$\mu^+ + \nu + \pi^\circ$	3.9 percent
6.	$\pi^+ + \pi^\circ + \pi^\circ$	2.15 percent

Modes 1, 2, and 4 cannot produce a charged decay product which can both pass through the counter telescope and have the proper range and dE/dx to be confused with a K meson. An upper limit was placed on the contributions of the remaining (three body) modes; in the following way: Assume a K meson is incident on the counter telescope and decays into three particles a distance x in front of the telescope. Let θ be the decay angle of a given charged decay product in the center of mass system of the K, measured with respect to the initial direction of the K. Its center of mass momentum is p, and in general will be distributed from zero to some p_{max}, determined by the total energy available. For a certain range of θ and p, the velocity and angle of the decay product in the lab will be such that it will be confused with a K by the telescope. Corresponding to each angle θ, then, there will be a small range of p for which the decay product will be K-like in the lab. For many values of θ, of course, p will be greater than p_{max}, and so these values of θ will not contribute. We may calculate an upper limit, then, by assuming an isotropic decay in the c. m., and also that all of the decay products coming off at an angle θ have exactly the right momentum p to be K-like in the lab system, subject to the

restriction that p is smaller than p_{max}. By integrating over x, the distance from the decay point to the counter telescope, it is possible to find an upper limit for the total decay correction from this type of event. Each type of event is then weighted by its branching ratio, and also by the number of charged decay particles emitted. The resulting upper limit is equal to 2.1 percent of the number of events that would reach the counter telescope if only K's that did not decay were detected. Two-thirds of this 2.1 percent come from events within 10 inches of the counter telescope. Since this is only a rather generous upper limit, and of the order of the uncertainty in the number R_d above, it was neglected in the total decay correction used to reduce the data. The value of R_d used was 0.317.

Absorption and nuclear elastic scattering corrections were made using the emulsion data on K^+ meson inelastic scattering from the 1958 CERN report (21), elastic scattering data of Bhowmik, et al (22) (also in emulsion), and differential cross sections in hydrogen measured by Kycia, et al (23). The inelastic data are given per nucleon, uncorrected for the Pauli effect in the nuclei, and may be used directly. It is interesting to note that this inelastic cross section in complex nuclei drops smoothly from about 10 millibarns at 100 mev to zero at zero mev, and since the K's measured in the present experiment have energies from about 85 mev down to zero mev, it is important to include this energy dependence of the K cross section in the absorption corrections.

The elastic scattering data was converted from emulsion to the various materials present in the path of the K mesons in the present experiment by assuming a Z^2/A dependence for the cross section per nucleus.

Calculation of the multiple coulomb scattering in F-1 and F-2 showed that, as is often the case, scattering out of the acceptance aperture of the spectrometer compensated for scattering in, within better than half a percent. Since the counters inside the counter telescope were quite close to each other, no correction was made for multiple scattering in the telescope itself.

The total correction for scattering and absorption combined was 0.957, so that only 4.3 percent of the K's were lost by these mechanisms.

Other corrections used were for the efficiency of the fast timing circuits, e_t (= 0.93), and the efficiency of the counter telescope, e_c. As mentioned earlier, the efficiencies of C-1, C-2, and C-3 were assumed to be unity, within fairly large uncertainties. These efficiencies were, however, the same from run to run. The only contribution to the e_c, then, is that arising from the fact that some of the K's stopping in C-3 were vetoed by having one of their charged decay products pass out through C-4. The probability that this would happen could be calculated fairly accurately, since enough absorber had been placed between C-3 and C-4 that only products of the two body decays could reach C-4, and all these

would give a pulse in C-4 at least as high as a pion from the hydrogen target, and were thus certain to veto their parent K. So by averaging the solid angle subtended by C-4 over the region of C-3 in which K's were stopping, it was possible to find the fraction of the incident K's that were vetoed by C-4. This fraction was 0.274, therefore e_c is 0.726.

Combining all the corrections above gives R equal to 0.204.

D. Computation of Cross Sections

Table III lists the various total counting rates measured, along with the relevant below threshold rates. Errors shown are from counting statistics only. The below threshold rates for the Σ° runs are derived from the Λ° run at the same lab angle. The quantity $C(E_o)$ is the difference of $C_t(E_o)$ and $C_b(E_o)$, where $C_t(E_o)$ is the total counting rate at E_o. Two values of $C_b(E_o)$ are shown for the 1161 mev Σ° point, one being the measured value, and the other a value calculated from the known value of the cross section for Λ° photoproduction (5) and the measured below Λ°-threshold background. This was done because experimental difficulties that were not discovered until the experiment had been completed made it necessary to throw out a large block of data taken at the 37.5° Λ° point. Poor statistics resulting from lack of data at this point seriously limit its usefulness as a below

TABLE III

Summary of Counting Rates for K Meson Runs (per Kilobip)

Process	Λ°	Λ°	Λ°	Λ°	Σ°	Σ°	Σ°
k (mev)	1013	1108	1209	1311	1161	1269	1383
θ_{lab}	37.5°	50.9°	60.9°	68.9°	37.5°	50.9°	60.9°
E_o (mev)	1100	1200	1300	1400	1300	1400	1500
E_o^* (mev)	900	1000	1100	1100	1100	1200	1300
$C_t(E_o)$	9.06±2.08	5.05±.42	3.32±.35	3.30±.49	9.75±.67	7.44±.46	4.03±.58
$C_b(E_o)$	3.17±1.20	1.36±.39	2.02±.39	1.54±.41	7.86±1.80	4.34±.36	2.96±.31
					7.21±1.03 (calculated)		
$C(E_o)$	5.89±2.40	3.70±.57	1.29±.53	1.76±.64	1.89±1.92	3.10±.58	1.06±.64
					2.54±1.23 (calculated)		

threshold measurement for the Σ° point at 37.5°, so a value for the Σ° cross section at this lab angle was also computed using the known Λ° cross section.

Our equation for the cross section has now become:

$$\sigma(k,\theta') = C(E_o)\left[\frac{W\,B(E_o, k/E_o)}{k E_o}\,G(p,k)\right]^{-1} \times 1.67 \times 10^{-22}$$

where W, k, and E_o are in mev, and $\sigma(k,\theta')$ is in cm^2/steradian. In Table IV the values used for the various quantities in this equation are listed along with the results obtained for $\sigma(k,\theta')$. Errors quoted are from counting statistics. In addition, the absolute magnitudes of the cross sections stated may be as much as 15 percent too low due to the uncertainty associated with the efficiency of the counter telescope.

TABLE IV

Cross Section Calculations

Process	Λ°	Λ°	Λ°	Λ°	Σ°	Σ°	Σ°
k (mev)	1013	1108	1209	1311	1161	1269	1383
θ_{lab}	37.5°	50.9°	60.9°	68.9°	37.5°	50.9°	60.9°
$p_{c.m.}$ (mev)	202.7	283.3	350.1	407.2	213.5	298.7	369.0
$\theta_{c.m.}$	108°	120°	127°	134°	117°	125°	132°
E_o (mev)	1100	1200	1300	1400	1300	1400	1500
$B(E_o, k/E_o)$	.856	.855	.848	.838	.874	.869	.855
$W(E_o)$ $\frac{mev}{Kilobip}$	$.8743 \times 10^{-9}$	.8647	.8576	.8535	.8597	.8518	.8451
G(p, k)	8.05	6.49	5.88	5.66	8.04	6.46	5.87
$C(E_o)$	5.89±2.40	3.70±.57	1.29±.53	1.76±.64	1.89±1.92	3.10±.58	1.06±.64
					2.54±1.23 (calculated)		
$\sigma(k, \theta)$ $\frac{cm^2}{ster}$	1.81±.74 $\times 10^{-31}$	1.71±.26	0.789±.32	1.33±.48	0.785±.80	1.92±.35	0.867±.54
					1.050±.50		

V. THEORY

A number of authors have presented theoretical considerations on the photoproduction of K mesons near threshold which might permit one to determine the parity of the K-Λ and K-Σ systems relative to the nucleons (24-31). Some of this work has been through a perturbation approach, based on either the Born approximation applied to meson field theory (24-27), or on the "atomic model" in which the K - Y state is regarded as a real bound state (28). Moravscik has discussed a method for determining the KYN coupling constants and parities from the photoproduction data using the value of the residue at the pole in the unphysical region (29). This pole arises from the meson current (or retardation) process and is expected to be present on rather general grounds, independent of the validity of perturbation theory (32). More recently, the initial stages of an analysis of K photoproduction in the Mandelstam representation using the dispersion theoretic methods of Chew et al. have been discussed (30). All of these approaches suffer at present from the fact that the anomalous magnetic moments of the hyperons are not known, and also from the lack of data on any of the K photoproduction processes except those in which a positive meson is produced.

By expanding the expressions for the differential cross sections given by perturbation theory (24), Capps (26) has

shown that it is possible to represent the center of momentum differential production cross section by:

$$\sigma(k,\theta) = \frac{p}{Y} \; D \left\{ A + B \frac{p}{Y} \cos\theta + C \frac{p^2}{Y^2} \frac{\sin^2\theta}{(1 - \beta_k \cos\theta)^2} \right\} + \ldots$$

where p is the momentum of the K^+ meson produced, Y is the rest mass of the hyperon, A, B, and C are dimensionless functions of the various rest masses and effective anomalous moments, and for convenience D is chosen to be: *

$$D = \frac{1}{4} \frac{e^2}{4\pi} \frac{G_Y^2}{4\pi} \frac{Y^2}{X W^2 k} \; .$$

In this expression, $e^2/4\pi = 1/137$, G_Y is the KYN coupling constant, K is the rest mass of the K meson, X is $Y + K$, W is the total energy available in the center of mass system, and k is the center of mass momentum of the incoming photon. If we denote the proton rest mass by M and the effective hyperon anomalous moment in nuclear magnetons by μ, then:

---

*D is given in units where $\hbar = c = 1$.

$$A = \left[1 + \mu\left(\frac{M \pm X}{2M}\right)\right]^2$$

$$B = \left[1 + \mu\left(\frac{M - X}{2M}\right)\right]\left[1 + \mu\left(\frac{M + X}{2M}\right)\right]$$

$$C = \left[(M \pm Y)^2 - K^2\right]\left[\frac{2X^3\, Y}{(X^2 - M^2)\, K^2}\right]$$

(Throughout this section wherever a choice of sign appears, the convention is used that the upper sign holds for scalar KYN parity, while the lower sign holds for the pseudoscalar case.) In the above expansion all terms of order higher than p^3 and some terms of order p^3 that are small compared to the last term shown have been neglected.

For $K - \Lambda$ production, the effective moment is given by:

$$\mu = \mu_p \pm \mu_\Lambda \pm \left(\frac{G_\Sigma}{G_\Lambda}\right) \mu_T$$

and for $K - \Sigma^\circ$ production, by:

$$\mu = \mu_p \pm \mu_{\Sigma^\circ} \pm \left(\frac{G_\Lambda}{G_\Sigma}\right) \mu_T$$

where μ_p, μ_Λ, and μ_{Σ° are the anomalous moments of the proton, Λ, and Σ° respectively. The transition moment $\mu_T = \langle \Sigma^\circ | \mu | \Lambda^\circ \rangle$ arises from Feynman diagrams with an internal hyperon line for which the hyperon is different from the hyperon in the final state. The Σ° - Λ relative phase is chosen in such a way that μ_T is a non-negative real number.

Assuming that the anomalous hyperon moments result exclusively from charge independent interactions of pions and Λ and Σ hyperons, Capps has shown that $\mu_\Lambda = \mu_{\Sigma^\circ} = 0$, and that $\mu_{\Sigma^+} = \mu_{\Sigma^-}$. If, in addition, global symmetry is required, then $\mu_T = \mu_{\Sigma^+}$. Marshak et al., using the mass differences of the hyperons (33), and Feld and Costa (28), using a model of Goldhaber's (34), have calculated various sets of these hyperon moments, and find $\mu_\Lambda = \mu_{\Sigma^\circ}$ in each case. In a paper on the lifetime of the Σ° (35), Dreitlen and Lee using dispersion theoretic methods similar to those used by Frazer and Fulco in their work on the nucleon form factors (36), find $\mu_T \simeq 0.64 \frac{g_\Lambda g_\Sigma}{g^2} \left(\frac{\mu_p - \mu_n}{2} \right)$ where g is the pion nucleon coupling constant, and g_Λ and g_Σ are the pion lambda and pion sigma coupling constants, respectively, and μ_n is the neutron anomalous magnetic moment. Little more is known about the effective moments, so that they, as well as the sign

and magnitude of each of the KYN coupling constants, must be treated as parameters in making a perturbation theory fit to the experimental data.

Let us examine the coefficients A, B, and C in more detail. A represents the S-wave production term resulting from the absorption of a magnetic (electric) dipole photon if the K meson is scalar (pseudoscalar). The first term in A corresponds to interaction with the magnetic Dirac (electric dipole) moment of the particles, while the second term is a "recoil correction" coming from the interaction of the absorbed photon with the effective anomalous moment of the system. Notice that this correction is largest in the scalar case, where a magnetic dipole photon is necessary for S-wave production. In general this recoil term is not small. The coefficient B corresponds to interference between the spin flip P-wave production amplitude and the (spin flip) S-wave term. The relationship between μ and the size of this interference term is of some interest. For B to be small compared to A, it is necessary that μ be large and positive in the scalar case (B is zero at $\mu = 2.8$ for Λ production, and at $\mu = 2.5$ for Σ° production). For a pseudoscalar K, μ would have to be somewhat negative (B is zero at $\mu = -0.92$ for Λ's, and at $\mu = -0.88$ for Σ°'s). We will return to these remarks later when discussing the experiments.

The last term, C, represents the non spin flip P-wave "retardation term." Numerical values of C are given in Table V.

TABLE V

Dimensionless Coefficient of the Retardation Term

Process	Λ	Λ	Σ°	Σ°
KYN parity	+	-	+	-
C	51.0	-2.8	53.0	-2.2

As we can see, for scalar KYN parity the retardation term clearly dominates the expression for the differential cross section at moderate momenta unless the effective moments are large, in which case A is also large. If μ is not too large, then, we can make use of the fact that C does not depend on μ to do a Moravscik extrapolation of the angular distribution data and thus determine the KYN coupling constant for the process involved. This method of measuring the KYN coupling constant has the advantage that it does not require a knowledge of the value of μ, provided of course that μ is small enough for the method to work at all.

To summarize the perturbation predictions, then, we can say: 1) in the scalar case, the retardation term will dominate the cross section not far above threshold if μ is small; if μ is large the S-wave term coming from magnetic dipole absorption will be large near threshold with the retardation term appearing at higher energies, and the cos θ interference term will be small; 2) in in the pseudoscalar case the S-wave term coming from electric dipole absorption will be large unless μ is between about one and four nuclear magnetons; an appreciable interference term will be present unless μ is near -0.9, the sign of this interference term will be negative if μ is less than -0.9 or greater than 2.8, otherwise it is positive; the retardation term should become noticeable if μ is between one and four but of course, since this term is negative for pseudoscalar K's, it can never completely dominate the cross section.

In analyzing pion photoproduction it was possible to use unitarity arguments to relate the data to data from the pion nucleon scattering measurements. These arguments are not particularly enlightening when applied to K photoproduction, for several reasons. For one thing, the photoproduction final states are related to K - hyperon scattering states, not to the observable K - nucleon scattering process. Even if this difficulty were overcome, there is the complication that the K photoproduction channel is not the only

one open, since production of single and multiple pions and also some of the new mesons is energetically permissible.

If there are any reactions which may be compared with the K^+ photoproduction data, they are the mesoproduction processes:

$$\pi^+ + n \rightarrow K^+ + \Lambda^\circ$$

$$\pi^+ + n \rightarrow K^+ + \Sigma^\circ$$

and more remotely:

$$\pi^- + p \rightarrow K^\circ + \Lambda^\circ$$

$$\pi^- + p \rightarrow K^\circ + \Sigma^\circ$$

These reactions have final states with the same isotopic spin as for the photoproduced K's. Only for the latter two reactions have a significant amount of data been accumulated (37). The data indicate that there may be a partial resonance in the isotopic spin 1/2 state at about the energy of the third pion nucleon resonance. This latter resonance is in an isotopic spin 1/2, $F_{5/2}$ state, and it appears unlikely at present that a state with such high angular momentum can contribute to the resonance in K mesoproduction, since the K "resonance" lies only 130 mev above the mesoproduction threshold. Still, it is possible that an $F_{5/2}$ resonance interfering with a large S and P-wave part could produce the observed results. Far above threshold, S and P-waves alone describe the K mesoproduction data quite well.

Some authors have suggested other resonances to explain the behaviour of the $\pi^- + p \rightarrow K^\circ + Y^\circ$ cross sections: Gourdin and Rimpault (38) and Tiomno et al. (39) have made calculations assuming the existence of a $K - \pi$ bound state, the K^* particle, while Kanazawa has postulated a $j = 1/2$ or $3/2$ resonance in $K - \Lambda$ scattering and has been able to fit some of the data reasonably well with his model (40).

There seems little to be learned at present from a comparison of the existing photoproduction data with these various resonance speculations.

VI. INTERPRETATION

The differential cross section data obtained in this experiment are shown in figs. 17 and 18. For comparison, two data points obtained earlier in the same range of center of mass angles as the present data are also included in the above diagrams. These points, one for the Λ reaction and the other for the Σ° reaction, were both obtained at Cornell, and are the only data available in this region other than the results of the present work. (7, 8, and 9). In fig. 17 is plotted also, for comparison, the average value of the angular distribution of the Λ cross section at 1000 mev photon energy as measured by Brody, Wetherell, and Walker (5). In forming this average it was assumed that the cross section was isotropic at this energy, as suggested by the data.

In fig. 17, the straight line represents an S-wave fit to the available data below 1060 mev photon energy, as given by Turkot at the 1960 CERN conference (8). The curve labeled "P. S." is based on a calculation using perturbation theory, and is discussed below. The straight line in fig. 18 is an S-wave fit to the Cornell Σ° data, also given by Turkot. The curves labeled "S." and "P. S." are again perturbation theory results and will be discussed below.

No previous data exists in the photon energy region explored by this experiment except at the extreme low end of the

FIGURE 17

CROSS SECTIONS FOR THE PROCESS $\gamma + p \rightarrow K^+ + \Lambda^\circ$

The differential cross section in the center of mass system is shown as a function of the center of mass momentum. Each point is labeled with the center of mass angle at which it was measured. The curve labeled "P. S." represents the Born approximation to perturbation theory, for a pseudoscalar $K\Lambda N$ parity, with a coupling constant $G_\Lambda^2/4\pi = 2.5$, and an effective moment $\mu = 0$. The other curve represents an S-wave fit to previous data, as given by Turkot (see text).

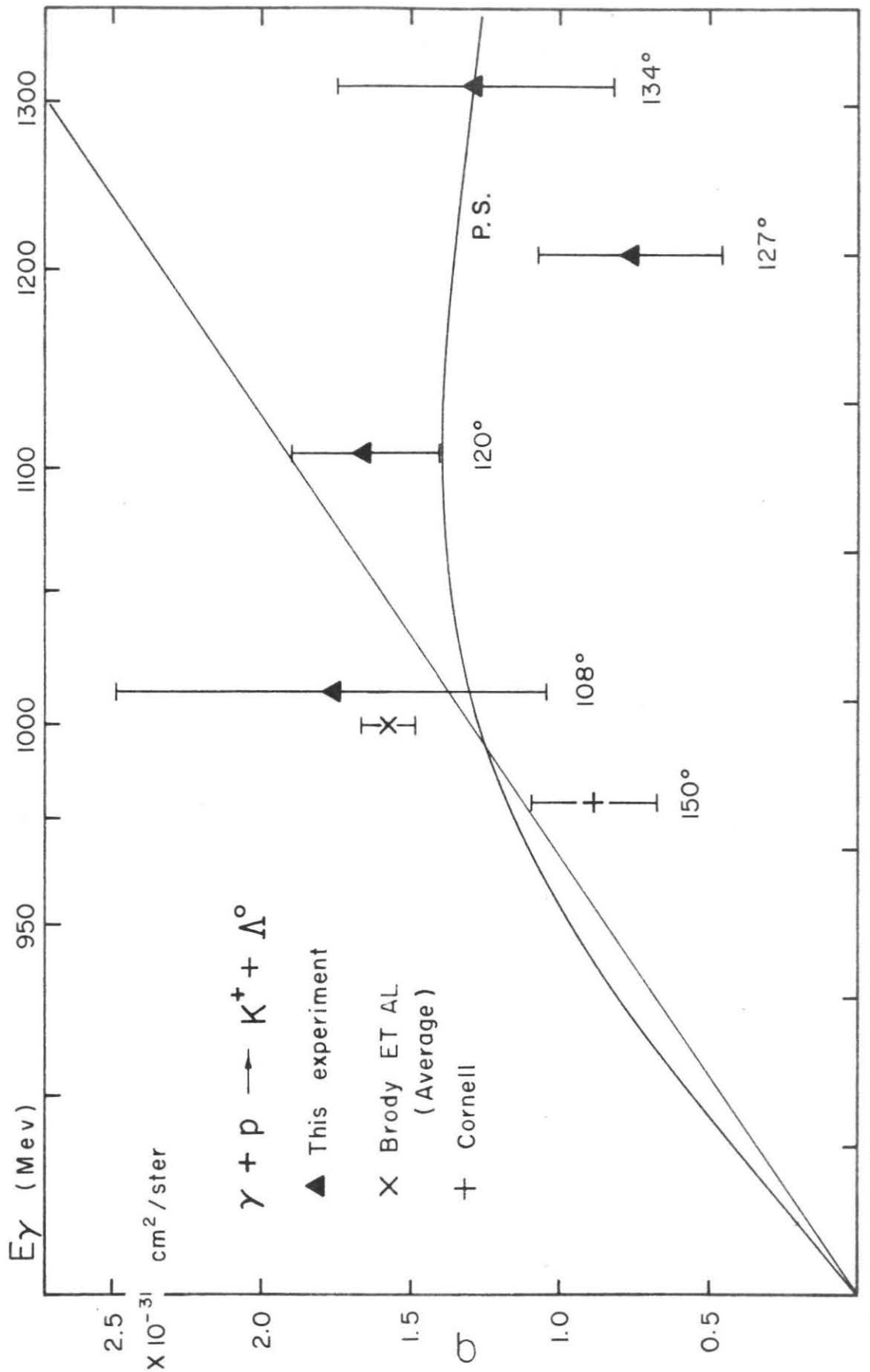
Eγ (Mev)
950
1000
1100
1200
1300
σ
X 10⁻³¹ cm²/ster
2.5
2.0
1.5
1.0
0.5
0
50
100
150
200
250
300
350
400
P'c.m. (Mev/c)
γ + p → K⁺ + Λ°
▲ This experiment
X Brody ET AL (Average)
+ Cornell
P.S.
108°
120°
127°
134°
150°

FIGURE 18

CROSS SECTIONS FOR THE PROCESS $\gamma + p \rightarrow K^+ + \Sigma^\circ$

The differential cross section in the center of mass system is shown as a function of the center of mass momentum. Each point is labeled with the center of mass angle at which it was measured. The curve labeled "P. S." represents the Born approximation to perturbation theory, for a pseudoscalar $K\Sigma N$ parity, with a coupling constanc $G_\Sigma^2/4\pi$ equal to 2.8, and an effective moment $\mu = 0$. The curve labeled "S." represents a similar approximation, assuming the $K\Sigma N$ parity is scalar, and $G_\Sigma^2/4\pi = 1.4$, while $\mu = 0$. The other curve represents an S-wave fit to previous data, as given by Turkot (see text).

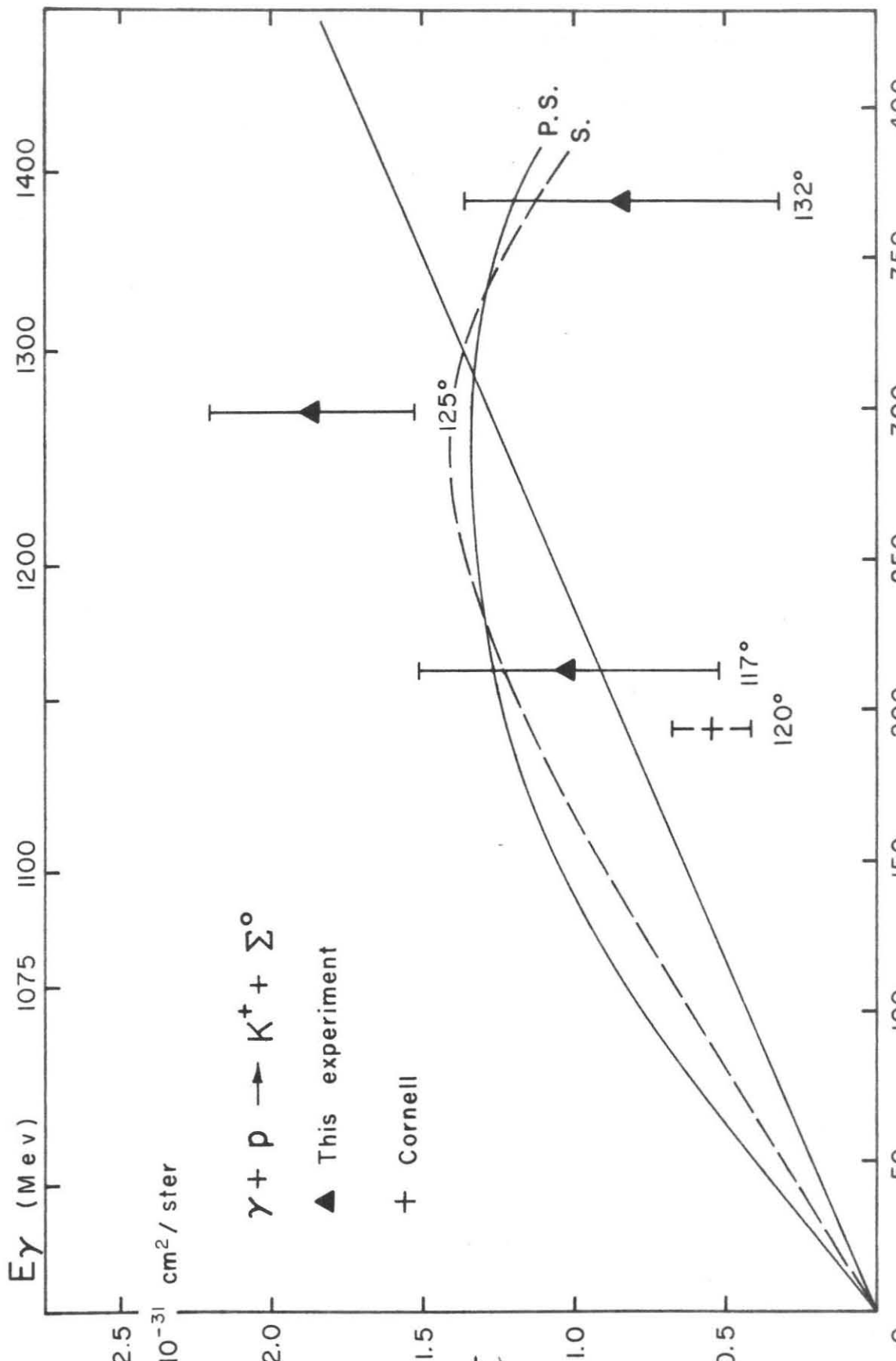
Eγ (Mev)
1075
1100
1200
1300
1400
2.5
x10⁻³¹ cm²/ster
2.0
1.5
1.0
0.5
0
σ'
γ + p → K⁺ + Σ°
▲ This experiment
+ Cornell
P.S.
S.
125°
132°
117°
120°
50
100
150
200
250
300
350
400
P'c.m. (Mev/c)

range, so that no comparison with existing angular distributions is possible except at the two lowest energy data points, where the present results are consistent with earlier work. The most noticeable feature of both the Λ and the Σ° excitation curves is that they are roughly similar in shape and in magnitude, and in particular, both curves begin to level off or even decrease slightly above a center of mass momentum of around 250 mev, dropping below the values that would result from simply extrapolating the low energy S-wave fits.

The remainder of this chapter will concern itself with a comparison of the K photoproduction data with the results of perturbation theory. This is the only theory presently available which makes sufficiently detailed predictions for such a comparison to be meaningful.

For reference, a table of the values of the various coefficients A, B, and C mentioned in chapter V is given in Table VI. The relative values of the coefficients are seen to depend heavily on the value of μ. Near 1000 mev photon energy, where most of the data on K - Λ photoproduction has been taken, p/Y, the center of mass momentum in units of the hyperon mass (Y is the mass of the lambda in this case), is about $1/6$, while $(p/Y)^2$ is about $1/40$, so that the interference term in the cross section should be noticeable if $B/6$ is of the order of A. Similarly, the effects of the

retardation term should appear if A is of the order of or smaller than C/40.

Although there may be a small positive interference term present, no appreciable retardation term is apparent in the existing Λ° data. Thus, either μ is large, and the K - Λ system is scalar, or μ is small ($|\mu| \lesssim .9$) and the K is pseudoscalar.

TABLE VI

Values of the Coefficients A, B, and C Calculated from Perturbation Theory

Process	KYN Parity	μ	A	B	C
		-3.6	14.8	-8.8	51.0
		-1.8	2.0	-2.3	
Λ	+	0	1.0	1.0	
		1.8	11.7	1.2	
		3.6	34.2	-1.6	
		-3.6	5.2	-8.8	-2.8
		-1.8	2.7	-2.3	
Λ	-	0	1.0	1.0	
		1.8	0.13	1.2	
		3.6	0.08	-1.6	
		-3.6	16.3	-9.8	53.0
		-1.8	2.3	-2.6	
Σ°	+	0	1.0	1.0	
		1.8	12.4	1.0	
		3.6	36.0	-2.7	
		-3.6	5.9	-9.8	-2.2
		-1.8	3.0	-2.6	
Σ°	-	0	1.0	1.0	
		1.8	0.08	1.0	
		3.6	0.19	-2.7	

The Cornell group, using Capp's values for μ, has made a perturbation theory fit to their $K-\Lambda$ data (7). They find $G_\Lambda^2/4\pi = 0.063$ for $K\Lambda N$ even, $G_\Lambda^2/4\pi = 2.2$ for $K\Lambda N$

odd. The values of μ used were $\mu = 3.6$ for $K\Lambda N$ even, $\mu = 0$ for $K\Lambda N$ odd. The result of a similar fit to the present excitation curve using $G_\Lambda^2/4 = 2.5$, $K\Lambda N$ parity odd, is shown in fig. 17 as the curve labeled "P. S." This fit was made using $\mu = 0$. Values of μ appreciably larger or smaller than zero result in an interference term, B, that is too small compared to A to produce the dropping off in the excitation curve at higher energies. (Remember that at these large angles, cos θ is negative, so that a positive value of B implies a $- p^2$ term in the excitation function.) The scaler theory does not fit the excitation curve in fig. 17 at all if $|\mu|$ is chosen to be large, as is required by the absence of a retardation term in existing $K - \Lambda$ data at lower energies.

A similar situation exists for $K - \Sigma^\circ$ photoproduction, although here it is not clear whether there is a retardation term appearing in the low energy data or not. At present the entire evidence for the existence of a retardation term in $K - \Sigma^\circ$ photoproduction rests in one data point at 1140 mev and at 85° in the center of mass system (8). Sakurai (31) has used this point along with other Cornell data at 1140 mev (9) to argue for the scalarity of the $K - \Sigma^\circ$ system, and, in fact, by extrapolating the angular distribution by means of the expression given in the theory chapter above to the pole in the unphysical region at cos $\theta = \beta_K^{-1}$, has obtained an

estimate of the (scalar) $K\Sigma N$ coupling constant. His curve corresponds to the perturbation expression with $A = 1.0$, $B = 0.2$, $C = 53.0$, and $G_{\Sigma}^2/4\pi = 0.62$. This function is consistent with the present data within rather large experimental uncertainties, although this latter data would favor a somewhat higher value of the coupling constant, on the order of one. More high energy data at more forward angles than those measured to date are need to firmly establish the existence of a retardation term in $K - \Sigma^\circ$ production, however.

Perturbation fits to the $K - \Sigma^\circ$ excitation curve are shown in fig. 18 for both a scalar ("S.") and a pseudoscalar ("P. S.") $K\Sigma N$ system. In both cases, μ was chosen to be zero. Values of $|\mu|$ much greater than zero would not permit a satisfactory fit for either parity. The coupling constants used for $K - \Sigma^\circ$ fits were 1.4 (even parity) and 2.8 (odd parity).

If μ is considered to be a free parameter, then a perturbation theory approach to the analysis of the existing data on K photoproduction allows us to make the following statements. 1) the $K\Lambda N$ system is pseudoscalar, and its coupling constant is about 2.5; 2) if the retardation term observed in earlier $K - \Sigma^\circ$ data is actually present, the $K\Sigma N$ system is scalar, otherwise it is not possible to ascertain the parity of this system from K photoproduction data at present; 3) if $K\Sigma N$ is scalar, $G_{\Sigma}^2/4\pi$ is

between about 0.6 (from Sakurai's result) and about 1.4; if $K\Sigma N$ is pseudoscalar, then $G_\Sigma^2/4\pi$ is about 2.8; 4) in any case, the effective moment μ is small for both Λ and Σ photoproduction.

A small value of μ for <u>both</u> reactions conflicts with the assumption that the anomalous hyperon moments result exclusively from charge independent interactions of pions and Λ and Σ hyperons. This follows from the discussion in chapter V, since under the above assumption, we have

$$\mu = \mu_p \mp \frac{G_\Sigma}{G_\Lambda} |\mu_T|$$

for production and

$$\mu = \mu_p \mp \frac{G_\Lambda}{G_\Sigma} |\mu_T|$$

for Σ° production, where, as before, the upper sign goes with even KYN parity. McDaniel et al. (7), using the above assumption and the $K^- - \Lambda$ data alone found earlier that, whether the $K\Lambda N$ parity was even or odd, G_Λ/G_Σ was negative. Now, the present data rules out the even $K\Lambda N$ fit to the $K^- - \Lambda$ data so that if G_Λ/G_Σ must be negative, the $K\Sigma N$ parity must be even. Therefore from the above expression for μ, $\mu = \mu_p + \left|\frac{G_\Sigma}{G_\Lambda}\right| |\mu_T|$ for

$K - \Sigma^\circ$ production, and this value of μ it too large to allow a satisfactory perturbation fit to the $K - \Sigma^\circ$ data.

Other assumptions for μ can be made of course; one that would allow the $\Lambda\Sigma$ parity to be even, for example, is $\mu_{\Lambda^\circ} \simeq \mu_{\Sigma^\circ} \simeq -\mu_p$ and μ_T small (i.e., $\frac{g_\Lambda g_\Sigma}{g^2} \ll 1$ in Dreitlen and Lee's model of μ_T). In this case, μ is small both for $K - \Lambda$ and for $K - \Sigma^\circ$ photoproduction.

It is well to emphasize that all of these conclusions rest heavily on the validity of perturbation theory for interactions involving hyperons and K mesons.

VII. CONCLUSIONS

Photoproduction of K^+ mesons in hydrogen has been studied at essentially one center of mass angle, for the photon energy range from 1013 mev to 1311 mev for production in association with lambda particles, and for the photon energy range from 1161 mev to 1363 mev for production in association with sigma particles. Only one of the data points, that for the $K - \Lambda$ production cross section at 1013 mev, is in a region of photon energies where previous data existed, although earlier measurements on the $K - \Sigma^\circ$ cross section had extended to energies as high as 1140 mev.

For the first time, a clear cut deviation of the excitation curve from S-wave behavior has appeared in the data for $K - \Lambda$ production. This deviation can be attributed to the presence of a positive interference term between the S and P partial waves. First order perturbation theory will allow a fit to all existing $K - \Lambda$ data only if $K\Lambda N$ is a system with odd parity.

The present data on the $K - \Sigma^\circ$ reaction add three more data points to the six already reported from Cornell, and are consistent, within rather poor statistics, with this Cornell data. First order perturbation theory applied to the present $K - \Sigma^\circ$ data allows no new conclusion to be made about the $K - \Sigma$ parity, although it does require that the effective anomalous magnetic moment

μ for K - Σ° production be small. This conflicts with certain predictions of Capps relating the effective moments to the $K\Lambda N$ and $K\Sigma N$ parities.

Because of the lack of any detailed predictions from the various theories based on the possible effects of resonances or or the recent discovered mesons (ρ, ω, η, ζ, and K*) on K photoproduction, no attempt was made to compare the data with these theories. The existence of these effects may well invalidate any conclusions based on perturbation theory.

VIII. RECOMMENDATIONS

The direction which the measurements of K^+ photoproduction in hydrogen will take in the near future is apparent. Measurements at higher energies and more forward angles should be able to determine unambiguously the $K\Lambda N$ and $K\Sigma N$ parities. This has been one of the primary goals of the K photoproduction experiments since it first became possible to perform them. To date, difficulties resulting from low counting rates and high backgrounds have prevented the attainment of that goal. Higher photon beam intensities in the energy region up to 1500 mev should soon be available, and the counting rates achievable will no longer be an important limitation. The background problems, however, will become more severe as the velocity in the laboratory system of the detected K particles and that of the background pions and protons approaches the velocity of light.

Even with higher intensities available, there is little theoretical justification at present for obtaining statistically better data at large center of mass angles until the forward angle measurements are quite good. The predictions of perturbation theory for the differential cross sections in the large center of mass angle region depend very little on the K - hyperon parities. This is not true, of course, at more forward angles.

If changes in the theoretical or the experimental situation should make it desirable to improve the data at large center of mass angles, the method used for the present measurements should be quite suitable, especially if use is made of recent progress in photomultiplier tube design, and in data handling equipment.

APPENDIX I

SOLID ANGLE CALIBRATION

The solid angle was checked using positive pions. This run was made at a pion lab momentum of 225 mev /c and a pion lab angle of 60°, using a bremsstrahlung end-point energy E_o of 1090 mev/c. The positive pion yield has been measured at this point by Bloch (41). He expresses his results in terms of a yield σ^* where

$$\sigma^* = \int_0^{E_o} \frac{B(k/E_o,\ E_o)}{k}\ \sigma_{T,\theta}(k)\ dk$$

In this expression, $\sigma_{T,\theta}(k)$ is the differential cross section for producing a positive pion of lab energy T and lab angle θ from a photon of energy k. We can write the number of pions emitted per equivalent quantum into solid angle $\Delta\Omega$ and lab energy interval ΔT^* from a target containing $\frac{pN_o\bar{\ell}}{A}$ hydrogen atoms as

$$C = \frac{\rho N_o \bar{\ell}}{A}\ \Delta\Omega\Delta T^*\ \sigma^* \qquad (A-1)$$

To write this in terms of the central momentum of the spectometer, p_o, we note that $\Delta T^* = \frac{dT^*}{dp^*}\ \Delta p^* = \beta^* \Delta p^*$ and

$\Delta p^* = \frac{\Delta p^*}{\Delta p_o} \Delta p_o$, so

$$C = \frac{\rho N_o \bar{\ell}}{A} \left[\Delta\Omega \frac{\Delta p_o}{p_o} \right] \frac{\Delta p_o^*}{\Delta p_o} \; p_o \; \beta^* \; \sigma^*$$

or

$$\Delta\Omega \frac{\Delta p_o}{p_o} = \left[\frac{\rho N_o \bar{\ell}}{A} \frac{\Delta p_o^*}{\Delta p_o} \; p_o \; \beta^* \right]^{-1} \frac{C}{\sigma^*} \qquad \text{(A-2)}$$

The observed counting rate, C_o, must be corrected for pion decay and absorption, detection efficiencies, and electron contamination to obtain the true counting rate, C.

The decay corrections consist of two contributions, first, pions emitted into $\Delta\Omega\Delta T^*$ which decayed into muons before they were detected, and second, pions which decayed and which may or may not have been emitted into $\Delta\Omega\Delta T^*$, but whose decay muons passed through the detectors and registered as pions. Approximate methods for calculating these corrections have been worked out in this laboratory and the methods as well as explicit formulas are discussed by Bloch (41) and by Dixon (42). After allowance is made for a slight amount of absorption of pions in A-0, F-1, and F-2, these methods can be applied directly to the present case.

Absorption corrections were made assuming that whenever a pion underwent a nuclear interaction it was not detected as a

pion. The sole exception to this rule was that if a pion scattered through an angle less than 45° off hydrogen in the counter telescope material, it was assumed that the pion was always detected. Since little of the absorption correction was due to hydrogen in the telescope, the angle assumed is not critical. All total cross sections were assumed to be geometrical, which is a good approximation in the pion energy range of interest (around 110 mev). The differential cross sections in hydrogen were taken from the work of Anderson, et al. (43). The combined decay and absorption corrections can be expressed as:

$$R = R_{\mu} R_1 + R_{\mu} R_1 R_2 + R_{\pi} R_1 R_2 R_3 ,$$

where the definitions of the various constants are as given in Table A-I.

TABLE A-I

R	Ratio of pions actually detected to pions produced in in $\Delta\Omega\Delta T$*
R_{μ_1}	Ratio of decay muons created in first half of magnet path to pions produced
R_{μ_2}	Ratio of decay muons created in last half of magnet path to pions produced
R	Fraction of pions which do not decay before reaching the telescope
R_1	Fraction of pions absorbed in target, A-0, and F-1
R_2	Fraction of pions absorbed in F-2
R_3	Fraction of pions absorbed in counter telescope before C-4

The values used for these constants are given in Table A-II.

TABLE A-II

R	0.812
R_{μ_1}	0.054
R_{μ_2}	0.083
R_{π}	0.814
R_1	0.957
R_2	0.988
R_3	0.886

The uncertainty in R is about 2 percent, due to a 15 percent to 20 percent uncertainty in calculating R_{μ_1} and R_{μ_2}.

The electron contamination was not measured, since it had been measured in the experiment of Bloch, and was shown to be small. From examining Bloch's data, 3 percent of the "pions" could be ascribed to electron counts.

Detection efficiencies were determined by using a pulse height analyzer to display spectra of the signals from each of the counters and the "sum" signals from chronotrons I and II. The efficiency measured was 98 percent.

Enough oscilloscope pictures were taken to establish 4 percent counting statistics, and an empty target background run

was made. The observed counting rates per 10^9 equivalent quanta were:

Target full	10.42 ± 0.42
Target empty	0.416 ± 0.075
Net	10.00 ± 0.43

Applying the corrections mentioned above for decay, absorption, electron contamination, and detection efficiency, the true pion counting rate is then 12.20 ± 0.53 per 10^9 equivalent quanta.

The values of the variables in equation (A-2) that were used to compute $\Delta\Omega \frac{\Delta p_o}{p_o}$ are listed in Table A-III.

TABLE A-III

Quantity	Value
$\frac{\rho N_o \overline{\ell}}{A}$	2.970×10^{23} nuclei/cm^2
β^*	0.850
p_o	212.7 mev/c
$\frac{\Delta p_o^*}{\Delta p_o}$	0.950
σ^*	14.3×10^{-32} cm^2/ster

The target hydrogen density used was 0.0692 gm/cm^3. This is the difference between the full target density and the "empty" target density, and allows for the fact that 2.1 percent of the hydrogen is still present in the target during the "empty" target runs.

With the above data, $\Delta\Omega \frac{\Delta p_o}{p_o}$ is 0.00167 ± 0.00009 steradian. The uncertainty quoted takes into account counting statistics, the 2 percent uncertainty in the counting rate arising from the decay corrections, and the uncertainty in the value of σ^*.

Using information in Section VIII of the magnet report (15), along with the dimensions and positions of V-2 (the rear anti-scattering counter) and F-2 (the aperture counter,) it was possible to calculate the change in the value of $\Delta\Omega \frac{\Delta p_o}{p_o}$ due to the presence of these counters. The results of this calculation give $\Delta\Omega\frac{\Delta p_o}{p_o} = 0.00162 \pm 0.00004$ steradian.

The value of $\Delta\Omega\frac{\Delta p_o}{p_o}$ used in reducing the K meson data was taken as the weighted average of the above two numbers, or 0.00163 ± 0.00004 steradian.

REFERENCES

1. P. L. Donoho and R. L. Walker, Phys. Rev. 107, 1198 (1957).
2. P. L. Donoho and R. L Walker, Phys. Rev. 112, 981 (1958).
3. A. Silverman, R. R. Wilson, and W. M. Woodward, Phys. Rev. 108, 501 (1957).
4. H. M. Brody, A. M. Wetherell, and R. L. Walker, Phys. Rev. 110, 1213 (1958).
5. H. M. Brody, A. M. Wetherell, and R. L. Walker, Phys. Rev. 119, 1710 (1960).
6. B. D. McDaniel, A. Silverman, R. R. Wilson, and G. Cortellessa, Phys. Rev. Letters 1, 109 (1958).
7. B. D. McDaniel, A. Silverman, R. R. Wilson, and G. Cortellessa, Phys. Rev. 115, 1039 (1959).
8. F. Turkot (rapporteur), Proceedings of the 1960 Annual Conference on High Energy Physics at Rochester, 369 (1960), University of Rochester.
9. D. A. Edwards, R. L. Anderson, F. Turkot, and W. M. Woodward, Bull. Amer. Phys. Soc. 6, 39 (1961).
10. R. L. Anderson, F. Turkot, W. M. Woodward, Phys. Rev. 123, 1003 (1961).
11. P. L. Donoho, E. B. Emery, and R. L. Walker, Unpublished.

12. J. Boyden and R. L. Walker, Unpublished. (See also J. Boyden, Ph. D. Thesis, California Institute of Technology (1961)).

13. R. Gomez, private communication.

14. R. R. Wilson, Nuclear Instr. 1, 101 (1957).

15. J. Vette and W. Wales, Low Energy Magnet Report, (1957), Unpublished.

16. R. L. Garwin, Rev. Sci. Instr. 23, 755 (1952).

17. D. D. Elliot, Ph. D. Thesis, California Institute of Technology, 20-24 (1959).

18. T. J. Gooding and H. G. Pugh, Nucl. Instr. and Meth. 7, 189 (1960).

19. University of California Radiation Laboratory Staff, Counting Handbook, (1958), University of California Radiation Laboratory.

20. P. G. Hoel, Introduction to Mathematical Statistics, 177 ff. (1947), John Wiley and Sons.

21. M. F. Kaplon (rapporteur), 1958 Annual International Conference on High Energy Physics at CERN, 171 (1958), CERN, Scientific Information Service.

22. B. Bhowmik, D. Evans, S. Nilsson, D. J. Prowse, R. Anderson, D. Keefe, A. Kernon, and J. Losty, Nuov. Cim. 6, 440 (1957).

23. T. F. Kycia, L. T. Kerth, and R. G. Baender, Phys. Rev. 118, 553 (1960).

24. M. Kawaguchi and M. Moravcsik, Phys. Rev. 107, 563 (1957).

25. A. Fujii and R. Marshak, Phys. Rev. 107, 570 (1957).

26. R. Capps, Phys. Rev. 114, 920, (1959).

27. D. Amati and B. Vitale, Nuov. Cim. 6, 394 (1957).

28. B. Feld and G. Costa, Phys. Rev. 110, 968 (1958).

29. M. Moravcsik, Phys. Rev. Lttrs, 2, 352 (1959).

30. Fayyazuddin, Phys. Rev. 123, 1883 (1961).

31. J. Sakurai, Nuov. Cim. 20 1212 (1961).

32. J. Taylor, M. Moravcsik, and J. Uretsky, Phys. Rev. 113, 689 (1959).

33. R. Marshak, S. Okubo, and E. Sudarshan, Phys. Rev. 106, 599 (1957).

34. M. Goldhaber, Phys. Rev. 92, 1279 (1953); 101, 433 (1956).

35. J. Dreitlen and B. W. Lee, Phys. Rev. 124, 1274 (1961).

36. W. Frazer and J. Fulco, Phys. Rev. 117, 1603, 1609 (1960).

37. J. Steinberger (rapporteur), 1958 Conference on High Energy Physics at CERN, 147 (1958), CERN, Scientific Information Service.

37. (continued)

S. Wolf, N. Schmitz, L. Lloyd, W. Laskar, F. Crawford, Jr., J. Button, J. Anderson, and G. Alexander, Rev. Mod. Phys. 33, 439 (1961).

38. M. Gourdin and M. Rimpault, Nuov. Cim. 20, 1167 (1961).

39. J. Tiomno, A. Videira, and N. Zagury, Phys. Rev. Lttrs. 6, 120 (1961).

40. A. Kanazawa, Phys. Rev. 123, 997 (1961).

41. M. Bloch, Ph. D. Thesis, California Institute of Technology, (1957).

42. F. P. Dixon, Ph. D. Thesis, California Institute of Technology, (1959).

43. H. Anderson, E. Fermi, R. Martin, and D. Nagle, Phys. Rev. 91, 155 (1953).